

**Modelling the Lava Dome Extruded at Soufriere Hills Volcano, Montserrat,
August 2005 - May 2006**

Part I: Dome Shape and Internal Structure

A. J. Hale¹
E. S. Calder²
G. Wadge³
S. C. Loughlin⁴
G. A. Ryan⁵

1 School of Geosciences, The University of Sydney, NSW 2006, Australia

2 Center for Geohazards, State University of New York at Buffalo, USA

3 Environmental Systems Science Centre (ESSC), University of Reading, U. K.

4. British Geological Survey, Edinburgh, EH9 3LA, UK

5. Institute of Earth Science and Engineering, University of Auckland, 1142, New Zealand.

12th February 2009

Abstract

Lava domes comprise of core, carapace, and clastic talus components. They can grow endogenously by inflation of a core and/or exogenously with the extrusion of shear bounded lobes and whaleback lobes at the surface. Internal structure is paramount in determining the extent to which lava dome growth evolves stably, or conversely the propensity for collapse. The more core lava that exists within a dome, in both relative and absolute terms, the more explosive energy is available, both for large pyroclastic flows following collapse and particularly for lateral blast events following very rapid removal of lateral support to the dome. Knowledge of the location of the core lava within the dome is also significant for hazard assessment purposes. A spreading toe or lobe of core lava over a talus substrate may be both relatively unstable and likely to accelerate to more violent activity during the early phases of a retrogressive collapse. Soufrière Hills Volcano, Montserrat has been erupting continuously since 1995 and has produced numerous lava domes which have suffered collapse events. We consider one continuous dome growth period, from August 2005 to May 2006 that resulted in a dome collapse event on 20th May 2006. The collapse event lasted 3 hours, removing the whole dome plus dome remnants from a previous growth period in an unusually violent and rapid collapse event. We use an axisymmetrical computational Finite Element Method model for the growth and evolution of a lava dome. Our model comprises of evolving core, carapace and talus components based on axisymmetrical endogenous dome growth, which permits us to model the interface between talus and core. Despite explicitly only modelling axisymmetrical endogenous dome growth our core-talus model simulates many of the observed growth characteristics of the 2005 - 2006 SHV lava dome well. Further, it is possible for our simulations to replicate large-scale exogenous characteristics when a considerable volume of talus has accumulated around the lower flanks of the dome. Model results suggest that dome core can override talus within a growing dome, potentially generating a region of significant weakness and a potential locus for collapse initiation.

1. Introduction

Many siliceous lava domes are comprised of a malleable core, solid carapace and granular talus. It is the largely degassed carapace on the outer surface of the dome which provides the source of the clastic talus components. As a lava dome grows the carapace may become over-steepened

and collapse, breaking apart and generating talus which is deposited at the foot of the lava dome, and the structural domain it forms is the talus apron. Some lava domes tend to collapse and fragment easily (e.g. Soufrière Hills Volcano, Cole et al. 1998, Sparks et al. 1998, Calder et al. 2002, Wadge et al., 2008). Other lava domes tend to collapse less readily and form relatively minor talus aprons (e.g. Mount St Helens, 2004-2008, Vallance et al., In press; Major et al., In review), or have no/little propensity for collapse and have virtually no talus (e.g. Soufriere, St. Vincent, Huppert et al. 1982).

At the Soufrière Hills Volcano (SHV), Montserrat, the talus apron is known to be a volumetrically important component of the dome (Wadge et al., 2008). From the point of view of constraining extrusion rates, accounting for material that has been added to the dome and subsequently deposited into the talus apron is important. Also, from a hazard perspective, understanding what component of the dome comprises ductile continuous (gas-pressurized) core, and what volumetric component comprises fragmented, degassed debris, is an important consideration (Simmonds et al., 2005; Wadge et al., In revision). What is less well understood is what role the structural strength of the talus apron might play in resisting growth of the core or precipitating the sudden collapse of the core as a whole. The elastic nature of this material, as it sits juxtaposed to a growing core, may play an important structural role in dome stability, for example a buttressing effect, and conversely a point of weakness during periods of intense rainfall (Carn et al., 2004).

In this paper we focus upon a period of dome growth at the Soufrière Hills Volcano (SHV), from August 2005 to May 2006, which began with relatively slow growth, accelerated to a much faster growth rate, and ended in a wholesale collapse on 20 May 2006 (Loughlin et al., 2009). We attempt to constrain how the core-talus interface evolved during this period and determine whether continuum numerical models of this evolution can help to understand the eventual instability of the dome. We use an axisymmetrical Finite Element Method (FEM) computational model for lava dome growth, comprising of core, carapace, and talus components (Hale, 2008). The shear-thinning viscosity relationship of Lavallée et al. (2007) and Newtonian behaviour are used to represent the rheology of the lava. Observed dome profiles, and extrusion rates from the dome growth period are used to constrain the model and generate configurations of the dome

during its growth evolution. In particular, we use survey data for the shape of the dome collected by the Montserrat Volcano Observatory (MVO) and, for an 11-day interval in March – April 2006 when the AVTIS (All-weather Volcano Topographic Imaging Sensor) instrument measured the daily growth (Wadge et al., 2005; 2008). This instrument obtained information on the growth of one side of the dome and showed that the surface of the talus apron aggraded by approximately 2 m/day.

After summarising lava dome growth over the considered time-period in Section 2, Section 3 discusses the computational model and how the core, carapace and talus domains are represented internally. We use the observed extrusion rates to force the core-talus model to evolve over the whole period and discuss the results in Section 4 in terms of a comparison with the AVTIS-measured profiles (Wadge et al., 2008) and those measured by automated camera from February to May 2006. In a companion paper (Hale et al., 2009) we explore how the physical process of rockfalls, and their detection by the seismic network of MVO, can be related to the model results.

2. Lava Dome Growth

The internal structure of a lava dome is largely governed by the growth regime; which for SHV predominantly involves the transport of lava directly to the dome surface, near the summit, producing shear lobes and spines (Watts et al., 2002).. Localized mass wasting occurs largely from the carapace and headwall of these lobes, particularly as they move outwards and encounter steeper slopes (Calder et al., 2002). Less frequently, dome growth has been observed to be entirely endogenous with dome growth accommodated by the swelling of the core or via intrusion, which forces the crystal-rich surface to break apart and generate rockfalls from all regions on the dome surface. Aggregate dome growth is therefore a variable combination of the two end-member scenarios, endogenous and exogenous (Major et al., In review). Loughlin et al. (2006) (Figs. 25, 25) distinguished the different styles of dome growth, along with dome volume estimates from December 2005 to May 2006. An important point is that growth accommodated entirely endogenously occurs for relatively short periods of time, but during these periods large positive volume changes can be recorded.

Observational data for the internal structure of lava domes is limited. Nicollin et al. (2006) used geo-electrical measurements for the Soufriere of Guadeloupe lava dome to construct a geophysical image of its internal structure. They found that relatively stable units lie above a basal inclined layer of highly conductive geological material; interpreted to be altered rock and characterised by a reduced internal friction. They also show that the lava dome consists of several domains with relatively high resistance, separated by conductive channels. This is consistent with geological observations that the dome core is massive but cut by fractures. Herd et al. (2005) considered the lava dome collapse event that occurred on SHV in 2003 after approximately three and a half years of dome growth and inferred the internal structure of the lava dome from a series of photographic images taken of the growing lava dome obtained by digital camera. As a result, the location of shear lobes, spines and talus from one viewing angle has been mapped to approximate the dome internal structure, assuming no further lateral displacement of the structures occurred after being covered by talus. Just prior to collapse, Herd et al. (2005) estimated the core of the lava dome to be approximately 300 m wide and 400 m high and with a talus comprising of more than 50% dome volume. Wadge et al. (In revision) traced the boundary at the surface between the lava core and the top of the talus over three episodes of dome growth at SHV and concluded that the surface expression of the boundary moved very steeply outwards with time as the dome grew.

The August 2005 – May 2006 Dome

The dome grew within the amphitheatre left by the huge collapse of the previous dome that occurred on 12 - 13 July 2003 (Herd et al., 2005). The extrusion rate was low for the first 4 - 5 months, with an average of approximately $1.0 \text{ m}^3 \text{ s}^{-1}$, and then accelerated to values between 5 and $12 \text{ m}^3 \text{ s}^{-1}$ for much of the rest of the growth period (Loughlin et al., 2006). Dome growth involved a combination of internal swelling, spine growth, radial and asymmetric shear lobe development. For the first few weeks the predominant regime was endogenous growth of the whole dome. Following this, growth became dominated by shear lobe development (generally comprising both endogenous and exogenous growth), punctuated by periods of entirely exogenous or endogenous growth (Loughlin et al., 2006). Some pulses of high extrusion rate began with largely exogenous emplacement of sheet-like blocky lavas in the summit area,

closely followed by inflation of most if not all of the lava dome. In such cases, the inflated outer surface of the dome typically develops a fractured or herringbone structure (Fig. 1) and shows diffuse degassing. Endogenous growth of the entire lava dome was not observed after mid-January 2006 when the dome began to develop a long-lived compound structure. In general, dome growth at SHV is a combination of both endogenous core inflation and exogenous surface flow, as observed in typical shear lobes (e.g. Watts et al. 2002) and endogenous growth (inflation) of most of the dome is only commonly observed while domes are small (e.g. <20 Mm³ DRE in 2005 - 6).

The top of the conduit is situated in the upper western part of the crater at approximately 680 m above sea level (a.s.l.) (Loughlin et al., 2006) and the crater floor slopes away from the vent to the east (towards the open part of the crater wall and the top of Tar River valley Fig. 1). Largely as a result of this topography, shear lobes develop preferentially in the downslope direction i.e. to the NE, E and SE and the bulk of the dome/talus volume is also offset to the east relative to the top of the conduit. Active easterly-directed shear lobes can therefore volumetrically dominate the lava dome and this is an important observation in respect to the modelling that follows.

Immediately downslope of the vent feeding the SHV dome was a narrow ridge approximately 50 m high, a remnant of the earlier dome not removed during the 2003 collapse. This ridge buttressed the new growing dome, initially preventing downslope flow with a slope of about 12-15°. By November 2005 this ridge had been overtopped and a substantial talus slope began to develop to the east. Until the end of the growth period there were relatively few small-scale collapse events or explosions. The largest collapse-derived pyroclastic flow had a volume of approximately 2 Mm³, compared to the final collapse volume on 20 May 2006 of approximately 110 Mm³. Talus formation via rockfalls, however, was vigorous and produced a large talus apron within the crater. This suggests that the surface of the dome (the talus/carapace) was largely degassed but may have encased a volatile-rich core. Wadge et al. (2008) estimate that between 30th March 2006 and 9th April 2006, 57% of the dense rock equivalent extruded lava was converted into talus, 21% was removed from the dome by pyroclastic flows, with only 22% remaining as core. This period of dome growth was probably not representative of the total dome growth period and would have been highly exogenous. Using a different approach Wadge et al.

(In revision) estimate dense rock equivalent volumes for the entire dome growth period to be 52 - 47% talus, 3 - 12% pyroclastic flow deposits and 45 - 41% core.

There was a tendency during Phases II (1998-2003) and III (2005-2007) of the current eruption at SHV for lava domes to grow to very large sizes before collapsing. This behaviour contrasts with the lava domes extruded between 1995 and 1998 (Phase I), which had moderate to large collapse events more frequently (Calder et al., 2005). It appears that more frequent collapses tend to create a more heterogeneous, compound structure to the lava dome that perpetuates further structural failures on earlier shear failure surfaces, while at later times in the eruptive history of the SHV, dome growth has favoured lobe extrusion at higher extrusion rates. Higher extrusion rates tend to reduce microlite crystal growth (Melnik and Sparks, 1999), which can result in the preservation of a higher volume melt fraction in the core lava.

The 20th May 2006 SHV dome collapse event was very energetic, completely removing the lava dome over a period of less than 3 hours, with approximately 80% of the dome removed during 40 minutes of intense retrogressive collapse that exposed the pressurized interior (Loughlin et al., 2006, In prep.). From this we can hypothesise that the core was relatively intact, i.e. there were fewer highly degassed talus layers or structural discontinuities within the dome which allowed piecemeal collapse and thereby prevented the collapse from eating further into the dome. There was no obvious build-up in overall seismicity in the hours or days before the event. However, there were several episodes of intense rainfall over the volcano prior to the collapse, which may have contributed to the initiation of the collapse of the dome (Loughlin et al., In prep). Two collapse events, July 2003 and March 2000, that are also suspected to be rainfall-induced, collapsed in a similar style to the 20th May 2006 event.

3. Computational Model

Conceptually, we divide the lava dome into three units; a relatively intact and ductile interior (the core), a largely degassed region of intact lava that remains attached to the core (the carapace), and a granular, friction-controlled, more distal region (the talus). The most distal products of dome growth – the pyroclastic flow deposits are ignored here. The dome model grows

endogenously, in that there is no explicit pathway for new batches of lava to reach the dome surface. As a consequence, this model is only suitable for considering lava dome growth that replicates the large-scale structure and not the fine-scale detail. Modelling localised and hence exogenous dome growth would require additional physics, such as the development and evolution of shear bands and flow discontinuities, whose initiation and evolution are poorly constrained (Hale and Wadge, 2008).

For our continuum model of lava dome growth with a talus we consider the evolution of two different materials: a ductile core and a frictional talus. The frictional talus component is also considered to contain degassed carapace material. The axisymmetrical Finite Element Method (FEM) computational model for lava dome growth developed by Hale (2008), comprising of carapace/talus and core components is used and the model domain is shown in Figure 2. Dome growth occurs on two time-scales: continuous dome expansion, via the addition of new lava into the molten core interior, and relatively instantaneous talus readjustments due the disintegration of the carapace and subsequent rockfalls. Because of the differences in the time-scales of these two processes it is possible to split the model into stages, a growth stage due to the addition of new lava, and a talus re-adjustment stage (Hale, 2008). Although the rheology of intact crystal-rich lava core is reasonably well understood (Lavallée et al., 2007), the rheology of the talus is less well-constrained. The rheology throughout the talus is not likely to be constant, but as the talus wedge grows thicker the more basal regions may become more tightly packed and behave differently to talus closer to the dome surface. However, for simplicity we model the deformation of the entire dome as a ductile fluid, due to the low Deborah number, and vary the viscosity within the core and talus regions, whilst the free surface of the talus is modelled as a purely frictional material that rests at an angle of repose. The model equations are formulated in an Eulerian framework and the parallelised finite element based PDE solver eScript/Finley is utilised (Gross et al., 2007). Modelling the free surface is of primary importance because it is here that the talus develops and large deformations can occur, which requires a reliable and robust technique that can cope with large deformations. For this, the level-set method is used to trace flow fronts and boundaries without distorting the model space/mesh (Hale et al., 2007).

We use a solidus pressure isobar to determine where core material turns into carapace/talus. This condition is used for two reasons. First, it is well known that as magma ascends and the pressure decreases, volatiles can be exsolved promoting crystallisation and solidification (Couch et al., 2003; Cashman and Blundy, 2002; Hort, 1998). Intermediate lava, such as the andesitic lava of SHV, is dominated by degassing-induced crystallisation with cooling being negligible during lava dome emplacement (Sparks et al., 2000). Therefore the solidus pressure can be used to mark the transition to a solid state (Simmons et al. 2005), and we simplify our model by assuming that only degassing-induced crystallisation contributes to the growth of solid lava, i.e. the carapace/talus, and neglect cooling. The second reason is that a transition to a solid state as described by the solidus pressure is relatively easy to implement computationally (Hale, 2008).

3.1 Model Formulation

During a single time-step for the model, we first calculate the velocity and pressure fields of the dome material, talus and core, and grow the dome accordingly. Next, the extent of the solid/core interface within the dome is re-calculated and the interface updated. The interface between the carapace/talus and lava core is identified using knowledge of the existing core region. The updated core region corresponds to where the dome has a pressure greater or equal to the solidus pressure and where the dome material was originally designated as core. The updated carapace/talus region corresponds to regions where the core has a pressure less than the solidus pressure or where dome material was originally designated as carapace/talus. This prevents talus from being converted back into core material if the pressure becomes greater than the solidus pressure, which does not happen in reality, hence the necessity for tracking this interface. Lastly, the clastic nature of the talus allows readjustments so that it becomes gravitationally stable. Hence, material that is sitting on a steep slope will readjust to its angle of repose, which entails the final stage of the model over one time-step. These sub-steps are repeated continuously to allow the lava dome to grow in time. See Hale (2008) for a thorough discussion of this model.

The axi-symmetric lava dome grows onto a horizontal base fed by lava from the conduit exit applied as a parabolic velocity field. The Reynolds number is defined as $Re = \rho_{lava}VL / \eta_{lava}$, where ρ_{lava} , V , L and η_{lava} are the density of the lava, characteristic velocity, characteristic length and viscosity, respectively. Defining V as the average velocity of a Hagen-Poiseuille flow in the

conduit, we estimate for SHV values for Re of the order 10^{-7} ; hence inertial effects can be safely neglected. In other words, for the present problem the lava is governed by the Stokes equations. The constitutive equation (given using Einstein notation) for a Newtonian, viscous material reads:

$$\sigma'_{ij} = 2\eta D'_{ij}, \quad (1)$$

where

$$\begin{aligned} \sigma'_{ij} &= \sigma_{ij} - P\delta_{ij} \quad \text{and} \quad P = -\frac{1}{3}\sigma_{kk}, \\ D'_{ij} &= D_{ij} - d\delta_{ij} \quad \text{and} \quad d = -\frac{1}{3}D_{kk}, \end{aligned} \quad (2)$$

and σ_{ij} is the stress, η is the viscosity, $D_{ij} = \frac{1}{2}(v_{i,j} + v_{j,i})$ is the stretching, δ_{ij} is the Kronecker delta and P the pressure. The Uzawa scheme is used to solve momentum equation 1, with the secondary condition of incompressibility, $-v_{i,i} = 0$, (for further details see Gross et al., 2007).

3.2 Lava Properties and Model Parameterisation

Our model requires several input parameters including: the viscosity of the lava in the core and talus regions, the extrusion rate or driving pressure, the solidus pressure, the friction angle for the talus, and the shape of the lava dome base (Hale, 2008). We parameterise the model with values appropriate for the August 2005 – May 2006 growth period on SHV, but the model is generic and can be applied to other volcanic systems. Dome growth is assumed to have begun at 00:00hr on 1st August 2005. Our simulation is initialised with a small mound of lava above the conduit vent corresponding to dome growth at a time of 0.45 days, a simulation start time of 10:48hr on 1st August 2005, and has a volume of 10,150 cubic metres (0.1% of the final dome volume). The lava dome collapsed on 20th May 2006; 292 days after the eruption began, and this corresponds to the end of the simulation. Dome growth is assumed to be axi-symmetric in a model space 450 m high and 500 m in the radial dimension. A first-order element type is used with an element

spacing of 2.5 metres. We now describe how we set-up and parameterise the model variables, and summarise these values in Tables 1 and 2.

3.2.1 Viscosity

The lava extruded at SHV contains abundant crystals and bubbles with a crystallinity estimated to be between 65% and 95% (Sparks et al., 2000). Lavallée et al. (2007) performed viscosity measurements on crystal-rich lava, resulting in a singular dependence of viscosity on the strain-rate regardless of the geochemistry, the crystal content, and up to 25% bubbles. We use the shear-thinning viscosity relationship without a yield strength as presented in Lavallée et al. (2007) for crystal-rich lava (Eqn. 3),

$$\log \eta_b = -0.993 + 8974/T - 0.543 \log \dot{\gamma}. \quad (3)$$

Where η_b is the effective viscosity in Pa s, T is the temperature in degrees centigrade (830°C is used in our model, from Barclay et al. (1998)), and $\dot{\gamma}$ is the strain rate. One limitation with this relationship is that as the strain rate goes to zero, the effective viscosity goes to infinity. We therefore use a minimum strain rate cut-off value of 10^{-5} s^{-1} . This corresponds to a maximum viscosity of $3.4 \times 10^{12} \text{ Pa s}$. It is appropriate to use this viscosity value derived from a strain rate cut-off because Caricchi et al. (2007) show that for strain-rates below 10^{-5} s^{-1} lava has a strain rate independent viscosity, hence in this regime the material behaves as a Newtonian fluid.

3.2.2 Geometry

From 1 August 2005 the lava dome grew on a surface that sloped to the east-northeast at about 12-15° with a restraining ridge just downslope from the vent, as described earlier. For computational simplicity we assume instead that the dome grew on a horizontal, flat surface and growth was essentially axisymmetrical, allowing us to model the dome using axi-symmetrical coordinates to significantly reduce the computer solving time.

3.2.3 Volume

The lava dome grew within English's Crater, which is open to the east-northeast. This means that pyroclastic flows and talus were constrained by the crater walls in all other directions until the

summit of the dome reach a height greater than approximately 960 metres above sea level (Wadge, 2009). Between 3 and 12% by mass of the dome was converted to pyroclastic flow deposits during this period, however we make no explicit account for this in the model. Mass-loss due to energetic pyroclastic flows may be an important process at later times in the growth of the dome and could be easily implemented into the dome model by adjusting the dome free-surface. However, without detailed observations of this process it would be inappropriate to introduce this variable into the model at this stage.

3.2.4 Density

The process of talus formation acts to increase the volume of talus compared to a unit volume of compact carapace. This volume change results in a density reduction; however, for simplicity we neglect any density change from core to carapace to talus in our simulation. The rheological properties of the lava dome may vary substantially within the dome. As the talus wedge gets thicker the more basal parts may increase in density and become stronger by pressure-induced tighter packing of clasts.

3.2.5 Extrusion Rate

Using the MVO survey data of the dome surface for the period August 2005 to May 2006, the volume change with time can be calculated. The process of talus formation increases the volume of talus compared to compact carapace or core and Wadge et al. (2008) used a ratio of 0.86:0.54 for core to talus densities to normalise the resultant volumes. But because we cannot account for separate core-talus volumes throughout this period we do not apply this here. In Figure 3 a best fit curve for the change in volume of the dome over time is applied and the cumulative volume V ($M m^3$) is approximated as:

$$V = 3.73 \times 10^{-6} t_d^3 + 2.76 \times 10^{-5} t_d^2 + 2.20 \times 10^{-2} t_d, \quad (4)$$

where t_d is the time in days. Using this best-fit volume-time relationship, the extrusion rate is obtained by taking the gradient, and this is used as the input for the model.

3.2.5 Talus Friction Angle

The angle of repose for the lava dome talus can vary spatially from being relatively steep (43 - 32°) near the carapace-covered core (Fig. 4), to less steep (<32°) more distally. These values are consistent with talus slope of 30 - 43.5° degrees measured by AVTIS during 2006 (Wadge et al., 2008). Our model has a fixed value for the talus angle of repose through the duration of the simulation, but we vary its magnitude between 37° and 43.5° in different simulations. Conventionally, it is assumed that the slope of the talus is considerably lower, approximately 33°, however, this appears not to have been the case at least during the August 2005 to May 2006 period measured. During the course of the eruption, the talus angle of repose has varied, and this variation is probably indicative of how the talus was deposited. For example, during shear lobe development, there are likely to be numerous energetic rockfalls or pyroclastic flows and the talus angle is likely to be lower than its critical angle of repose due to the additional kinetic energy associated with these flows (Lube et al., 2005). However, during periods when dome growth is predominantly endogenous or where there are fewer energetic rockfalls or pyroclastic flow, the talus will rest at angles closer to its critical angle of repose.

3.2.6 Solidus Pressure

For a dynamic system the solidus pressure or temperature is not likely to be a constant, but for simplicity we assume a fixed value. Observations of the carapace (e.g. Watts et al., 2002) indicate that it is only a few metres to a few tens of metres thick. This suggests that the solidus pressure can be relatively low. We assume that the solidus pressure lies within a range of 0.2-0.6 MPa (Table 1), which corresponds to a thickness range of about 4 - 21 m.

4. Results

We present results for our lava dome simulations using both a shear-thinning viscosity model (Lavallée et al., 2007) and a Newtonian viscosity model. The shear-thinning viscosity model uses a strain-rate cut-off value of 10^{-5} s^{-1} corresponding to maximum viscosity of $3.4 \times 10^{12} \text{ Pa s}$ for the lava core and talus (Eqn. 3). The Newtonian viscosity model uses a constant viscosity equal to $3.4 \times 10^{12} \text{ Pa s}$ for the lava core and talus (that is, a viscosity equal to the strain-rate cut-off value of 10^{-5} , Eqn. 3). We vary the solidus pressure and the friction angle since all the other parameters are relatively well constrained. We acknowledge that it may not be appropriate to model the talus

as having the same viscosity relationship as the core. In the talus fine-grained infill and incipient cementation may start to develop a cohesive strength. The 2D packing models of Wu et al. (2003, 2004) show that for both isostatic and directional compaction modes, the density (compaction) increases rapidly at low stress increments from about 0.6 to 0.9, but requires much higher stresses to reduce the last 10% porosity to zero. The reduction of porosity by rotation, grain deformation and fine grain infill will increase grain contact surface area and hence bulk friction coefficients. Thus there is evidence to suppose that the internal friction of the talus increases and to account for this change in bulk system properties we can increase the strength of the talus with respect to the core properties. Therefore, we also simulate dome growth using a shear thinning, strain-rate dependent, viscosity relationship (Eqn. 3) with a strain-rate cut-off value of 10^{-5} corresponding to maximum viscosity of 3.4×10^{12} for the lava core. The talus is modelled to have a viscosity ten to thirty times higher than the maximum cut-off viscosity used for the core.

4.1 Dome Surface

We use our model to consider the free-surface shape of the lava dome as well as the evolving maximum height and radius and compare them to observational data.

4.1.1 Lava Dome Free Surface on 30th March and 7th April 2006

A comparison of the simulated lava dome free-surface to the surface of the dome imaged from the north-northeast by the AVTIS device on 30th March and 7th April 2006, (Wadge et al., 2008) is presented (Fig. 5). Figure 5a shows the lava dome free-surface for shear-thinning and Newtonian viscosity models as described in Table 3. The Newtonian viscosity model produces a more conical shaped dome with a higher summit height and slightly smaller radial extent when compared to the shear thinning viscosity model. Figure 5b shows model results using a shear thinning viscosity model for three models with talus angles of repose equal to 37.0 °, 40.0 ° and 43.5°. A friction angle of 43.5° produces results that are closest to the lava dome free-surface imaged by Wadge et al. (2008). Figure 5c shows that changing the solidus pressure has very little effect upon the free-surface shape of the lava dome. However, introducing a higher viscosity for the talus region, a viscosity ten times higher than that of maximum possible core viscosity, results in the summit of the lava dome becoming lower, wider and flatter (Fig. 5d). For all of the

results presented in Figure 5, using a talus angle of repose equal to 43.5° produces the best fit to the dome free-surfaces on these dates. Changing the solidus pressure does little with respect to influencing the dome free-surface, except slightly changing the summit height (Fig. 5b). Varying the viscosity relationship changes the height of the dome in the summit region. A Newtonian viscosity model results in a summit region that is highest and slopes most steeply, hence a more conical dome. While the computational model that uses a shear-thinning (Lavallée et al., 2007) viscosity relationship, but with a higher viscosity in the talus region, produces the flattest and widest summit profile.

For all the simulated lava dome free-surfaces in Figure 5, the summit region of the dome departs from the inferred flat surface in Wadge et al. (2008), since AVTIS cannot image the summit of the dome due to the grazing angle of view. However, since our core-talus model does not simulate explicit exogenous growth of lava at the summit it may be less likely to provide realistic results in this region. For example, the change in location and direction of the extrusion points of lava flow observed at the summit (Watts et al., 2002) will tend to broaden the summit area. Thus a detailed comparison of the model simulations with observations of the summit region morphology is currently unlikely to be productive.

Wadge et al. (2008) calculated that during the deployment of AVTIS, over the time-period 30th March to 9th April 2006, the free-surface of the talus grew upwards by approximately 2 metres per day. Our simulated dome results produce a slightly lower range, approximately 10 to 13 metres over the 8 day period, approximately 1.3 to 1.6 metres per day. This difference may result from two effects. First, Wadge et al. (2008) imaged the dome from the active side of growth and therefore the dome is likely to accumulate more talus due to the extruded lava being channelled into the field of view of AVTIS. Second, the model we use is axi-symmetrical and therefore the volume of talus is distributed equally around the dome whereas the lava dome on SHV was not perfectly axi-symmetrical at the time. Dome growth was primarily directed towards the east as discussed earlier which would result in a larger talus accumulation rate in this region.

4.1.2 Lava Dome Height and Radius

The maximum height and radius of the simulated lava domes with time for the different simulations (Table 2) are plotted in Figure 6. Model results are relatively close to the observational data available for the radius. However, the height of the dome as calculated by the simulation is typically larger than that observed. The most likely reason for this is because of the model's assumption of a flat base. In reality, dome material will have tended to move down the slope to the east therefore reducing the mass and height at the dome summit as a result. Apart from this offset in height values, both model and observations show a near-linear growth in dome height and radius with time. Assuming that the dome is approximately conical in shape its volume can be approximated by $V = \frac{1}{3}\pi r^2 h$. For the radius, r , to increase approximately linearly with time, the volume must increase approximately as t^3 , assuming that $r \approx h$. From Equation 4 it can be seen that the t^3 term will become dominant at later times in the growth of the dome as t becomes large, suggesting that r and h should become approximately linearly proportional to t .

4.2 Dome Structure

We now consider the changes to the internal structure throughout the 292-day evolution of the lava dome using eight separate simulations with a range of parameters (Table 2).

4.2.1 Evolution of the Core-Talus Boundary

3D visual representations of simulations (Table 2) the lava dome with a section cut-out at four stages in its growth, to show how the free-surface and core evolve with time are shown (Figure 7). At early times in the simulation, the core is relatively narrow and the dome shape near-conical. However, at later times, the dome core has spread laterally and the dome shape departs from being near-conical to having a wider central region.

4.2.2 Carapace Adjustment Location

For every time-step during the simulated growth of the lava dome, just following the sub-step in which the new injection of lava occurs, we calculate where the free-surface of the lava dome has an angle greater than that of the angle of repose. From this we can work out the smallest radius

from the centre of the dome, R_a , and height H_a , where the dome surface is unstable, and hence where the talus needs to be adjusted to rest at its angle of repose. Figure 8a shows schematically the location of R_a and H_a . In our simulations, the talus region of the dome above the core-talus interface with a radius less than R_a is not likely to move significantly during each time-step. This results in the free-surface of the dome in the region $0 < R < R_a$ sloping at angles below the angle of repose with minimal talus adjustment. Therefore, it may be better to class this region of the dome as carapace, because talus will only fragment during displacement. This central carapace is only a relatively small region and will have little impact upon the volume of core to talus discussed later. However, by reclassifying this area, the carapace in our model effectively extends to the surface. Figure 8b shows the shape of the growing lava dome at five dates: 1 Oct. 2005; 1 Dec. 2005; 1 Feb. 2006; 1 Mar. 2006 and 20 May 2006 with the regions of talus in the model better classified as carapace shaded as grey.

The evolution of core-talus boundary for the eight simulations is shown in Figure 9. The black continuous lines correspond to the core-talus interface, and the grey continuous lines corresponding to the free-surface of the dome, at five dates for each simulation: 1 Oct. 2005; 1 Dec. 2005; 1 Feb. 2006; 1 Mar. 2006 and 20 May 2006 (Fig. 9, left column). The core initially grows primarily vertically in these simulations, before spreading laterally later on. This forces the core region to become wider and the summit flatter with time. Lateral spread of the core at later times in the growth of the dome results in the talus spreading above a layer of talus, as well as some of the talus being displaced laterally. There is less lateral spread of the core for the simulations in which the talus is more viscous than the core (simulations 6 and 7). Also, for these simulations the summit of the dome is slightly wider and flatter.

Also shown in Figure 9 (right column), are the incremental values of R_a and H_a , shown as grey circles, corresponding to the point at which the talus departs from the angle of repose. There are several effects that contribute to the scatter in the results. First, to calculate the slope of the free-surface we must consider a region one element wide that surrounds the free-surface zero iso-surface to ensure that there are elements within this region that are close to the free-surface (Hale et al., 2007). Second, the finite spacing between elements and nodes means that when the free-

surface angle is calculated, the angle is only known within elements of the mesh. For this simulation, this corresponds to only knowing the free-surface angle at a radial spacing of every 2.5 metres (an interval of approximately 0.5% of the domain).

When R_a is small, talus adjustments extend from very close to the summit (or at the summit) to the lateral extent of the talus, meaning that the dome is approximately conical. However, at increasing values of R_a talus adjustments occur further from the summit, resulting in a dome shape that is less conical but wide and flat in the central region. Results from all the model simulations for a friction angle of 43.5° show that R_a and H_a values lie approximately 55° from the r-axis, suggesting that the dome partially develops a core region sloping at angles below the talus angle of repose as well as a talus apron at larger radii. Using a lower friction angle for the talus, the results for R_a and H_a stay relatively close to the z-axis, suggesting that the dome shape will be approximately conical.

Generally, for all the simulations, R_a and H_a increase approximately linearly with respect to each other. However, simulations with the highest friction angle of 43.5° show that H_a initially increases with R_a , but at later times may remain at the same value or slightly decreases for increasing R_a . This is because at later times the dome core bulges laterally at mid levels within the dome and not as much near the lower frontal edge or near the summit. The locations of R_a and H_a from the simulations (grey points) can be compared to the observed locations of the boundaries between talus and core (red points) for dome profiles between February and May 2006 and presented by Wadge et al. (In revision, Fig.1). The behaviour is quite similar for some simulation results (Fig. 9 right column). Typically, simulations that use a friction angle equal to 43.5° for the talus produce the best fit of R_a and H_a pairs to the observational data set. Also observe that at later times in the growth of the lava dome the observational data set also shows that H_a can decrease or remain the same as R_a increases.

The point where the talus departs from the angle of repose appears to be a good indicator for where the talus bounds with the carapace on the dome surface. However, these data may be a

poor indicator of where the core-talus interface is within the dome interior. As we see from Fig. 9, the internal shape of the core-talus interface can depart radically for simulations showing quite similar patterns of R_a and H_a . At some stages in the growth of the lava dome, the lateral extent of the core is three to four times the value of R_a bearing no relation to where the extent of the core/talus interface actually exists on the dome surface.

4.2.3 Velocity Field

The velocity field on day 262 of Simulation 2 is shown in Figure 10. The magnitude of the velocity at the dome surface is largest at distances between 100 and 200 m above the base of the dome, due to the boundary condition of no-slip at the base of the dome and the boundary condition of no-stress for the dome surface. Hence, dome core over-riding the talus is clearly evident. Since our simulation only considers axisymmetrical endogenous dome growth and cannot capture shear lobe channelling, it may be over-estimating the lateral spread of the core within the dome. However, even if shear lobe growth were considered exclusively in our simulation there is likely to be some amount of lateral spread of any ductile core region that exists within the dome due to gravitational spreading.

Not only does the core override some talus, but over the duration of the simulation the core-talus boundary spreads laterally and can also be displaced downwards (Figure 9 and 10). The downwards movement of the core-talus interface may act to compact talus below the core region of the dome, increasing stability. Alternatively, if compaction of the talus does not occur, then this overridden talus region could generate a weak region of the dome.

4.2.4 Core-Talus Interface on 20th May 2006

At the end of the growth period, marked by the 20 May collapse, the simulated lava dome free-surface and core-talus interface for the models described in Table 2 are shown in Figure 11. The free-surfaces of the simulated lava domes are all very similar with the largest variation due to the changes in friction angle for Simulations 4 and 5 (Fig. 11a). However the core-talus interfaces are considerably different between simulations (Fig 11b). The Newtonian viscosity model (Simulation 8) produces the largest amount of talus between the base of the dome and the core. This is because this viscosity model does not exhibit shear thinning that promotes lateral spread.

There is also considerably less lateral spread for the dome cores for Simulations 6 and 7 in which the viscosity is highest in the talus region. The results for the final core-talus interface and dome free-surface shape for all the simulations considered are shown in Figure 11c.

Using seismic (RSAM) data Loughlin et al. (In prep) calculated that approximately 9% of the dome volume collapsed during a preliminary build-up phase. Following this, the dome collapsed catastrophically and was associated with explosive decompression of the core (Loughlin et al., In prep), removing the entire dome, including additional remnants from previous dome growth periods. Like several of the other dome collapse events on SHV, this one was preceded by heavy rainfall. The recorded rainfall in central Montserrat was close to the critical level required as defined in Matthews et al.'s (2002) model for rainfall induced collapse and was probably significantly higher on the volcano (Loughlin et al. In prep). It is likely that rain water was channeled along the talus-crater interface, causing erosion at the margins of the dome next to the crater walls. This idea, coupled with simulation results showing that the core can override the talus, suggests that initial undermining in this way could destabilise a region of core that could then lead to the observed retrogressive collapse and explosions. Assuming that the 9% of dome volume collapsed during this build-up period was derived mainly from the talus (Loughlin et al., 2006), we can calculate the amount of dome talus required to be removed before penetrating the core. Assuming a conical shape close to the lateral extent of the dome, the volume, V , of dome material between a radius R_C , and the maximum extent of the dome, R_T , is given by;

$$V = 2\pi \tan \theta \left(\frac{R_T^3}{6} - \frac{R_T R_C^2}{2} + \frac{R_C^3}{3} \right). \quad (6)$$

We assume a lava dome with a talus angle of repose, θ , equal to 43.5° , as appears most suitable for this period of dome growth from our models, and observational data for a maximum radial extent for the dome of 475 metres is used. The total lava dome volume prior to collapse was approximately 101 million cubic metres, meaning that approximately 9 million cubic metres of material was removed during this preliminary build-up phase. Assuming that talus removal only took place to the open east of the dome (say a 120° section or $1/3$ of the dome, Fig. 1) then talus

material would need to be removed to a radius $R_C = 320$ metres. Our lava dome simulation results suggest that the core can extend a lateral distance from approximately 220 m to 400 m, depending upon the solidus pressure and viscosity relationship chosen (Fig. 11c). We have no direct observational evidence that such a process exists, however, but these results certainly support its feasibility.

4.2.5 Core Volume Fraction

At each time-step for the lava dome simulations we save the volumes of the dome, core and talus. Figure 12 shows the time series of core volume fraction for all the simulations considered. At the start of dome growth, the initial core volume fraction is approximately 0.3 for all the simulations. This is because initially talus can develop from all regions of the dome. However, at later times in the simulation, talus only forms primarily near the summit of the dome, meaning the volume fraction of core within the dome can increase to larger values. Also, due to the boundary condition of no-slip at the base of the dome, this promotes lateral spread of the core just above the base of the dome increasing the core volume fraction only later in the simulation.

Decreasing the solidus pressure increases the core volume fraction. For Simulation 1 the solidus pressure is 0.2 M Pa resulting in a final core volume fraction of 0.75, while for Simulation 3 the solidus pressure is 0.6 M Pa resulting in a final core volume fraction of 0.65. Increasing the angle of repose for the talus, while maintaining the other parameters constant (Simulations 2, 4 and 5), acts to decrease the core volume fraction since a greater volume of talus is required to surround a dome with a smaller talus angle of repose.

The simulation that uses a Newtonian viscosity relationship (Simulation 7) has a core volume fraction growth curve that is significantly different from the simulations using a shear thinning viscosity relationship. The final core volume fraction for the Newtonian viscosity relationship is approximately 0.6, compared to approximately 0.7 for the shear thinning viscosity relationship with all the other parameters the same. This is due to a greater lateral spread of the core for simulations using a shear-thinning viscosity relationship. The shear thinning viscosity relationship simulations with a higher viscosity in the core, Simulations 6 and 7 have much smaller core volume fraction than for the other simulations, with core volume fraction values

between 0.3 and 0.4. This is similar to the range of dense rock core fraction estimates made by Wadge et al. (2008) for the same growth period: 0.41 - 0.45. However, because we do not consider a density change between core and talus we may be underestimating the volume of talus generated. Calculating a final talus volume using the dense rock equivalent ratio 0.86:0.54 for core to talus, the final core volume fraction for the simulated lava domes at a day 292 ranges from 26 to 66%.

5. Discussion

Our computational lava dome model simulates some of the observed growth characteristics of the August 2005 to May 2006 SHV dome reasonably well. In one sense this is surprising, because for most of the growth period lava was transported to the surface of the dome via shear lobes including both exogenous and endogenous growth, whilst the model simulates growth by adding each new batched of lava only into the base of the dome in an endogenous manner. Exogenous lava dome growth is commonly described as the addition of lava to the central summit region of the dome (e.g. spines) and mass wasting on the flanks. However, at later times in our simulations when a considerable volume of talus has accumulated around the lower flanks of the dome, our endogenous lava dome model is in many ways similar to conceptual exogenous models. This is most prominent in the simulations in which a higher viscosity is used for the talus region of the dome with respect to the core, resulting in lava being preferentially channelled vertically where the talus or carapace region is thinner (Fig. 9f). Therefore, despite not explicitly modelling the physics associated with exogenous dome growth, our model replicates some of the large-scale behaviour associated with it.

Our lava dome model does have a mechanism, based on the angle of the free surface, to simulate a frictional-controlled talus. The actual mechanism of talus generation: pushing and toppling of fracture-bounded blocks of carapace lava onto slopes where gravity aids disaggregation can be viewed as a critical-angle problem too. The model raises the possibility of moving the position of the critical-angle instability and disaggregation to quite low on the talus slope because of the lateral spread of the core-talus interface (e.g. Fig. 9b). In the context of the axi-symmetric model this would be observed as a band of talus reactivation and perhaps measurable bulging all the way around the talus apron. The localised lateral displacement of talus and dome carapace has

been observed but not measured at SHV. This oversteepening of the dome/talus as it is pushed from behind by lateral spread of the core is more common at higher extrusion rates and tends to be directed by discrete shear zones (Watts et al., 2002; Loughlin et al., In prep). Directed endogenous growth (particularly in the southern part of the dome has caused gross surface deformation (e.g. Watts et al., 2002). At Mount St. Helens there is also evidence of simultaneous localised endogenous and exogenous dome growth and the lateral displacement of the talus (Major et al., In review; Vallance et al., In press). For SHV dome growth is dominated by emplacement of shear lobes to the east (i.e. SE-NE), and these may have a significant endogenous component.

From observations of the surface position of the carapace/talus boundary over three episodes of lava dome formation at SHV, including the one considered here, Wadge et al. (In review) showed that this evolving boundary may be steep and tends to dip towards the centre of the dome. This is a similar geometry to the one simulated here. Wadge et al. (In review) argued that the evidence from the exposed core-talus boundary after the 2003 collapse event was of a steep surface not far from the downward extension of the surface-measured boundary prior to collapse and hence that there was probably no more than about 100 m of lateral spreading of the core-talus boundary after burial. Our simulation results tend towards this evolutionary shape when the talus is more viscous and resistive to deformation than the core. However, our model does not account for any inherited material property variability such as from earlier, structurally isolated and more rigid parts of the dome which would also tend to inhibit lateral spreading.

Our work then raises this key question: What is the degree of lateral spreading of core lava in a lava dome and how might it be measured? Quantitative 3D survey observations of the core-talus boundary revealed by large, but partial collapse would be one way to measure this effect, but there are very few opportunities to do so. Real-time measurement of surface deformation of the talus adjacent to the spreading could be feasible using ground survey instruments such as AVTIS or ground-based InSAR (e.g. Casagli et al., 2008). However, a key issue in this regard is whether the rate of readjustment of existing talus and deposition of new talus from above would be sufficient to mask any morphological signal. Any upward-directed intrusion producing a protuberance through the carapace should be obvious and measureable. But a deformation of the

talus lower down on the dome by lateral expansion of the core may be of smaller amplitude. Passive rockfalls (as defined by Calder et al., 2002) forced by the deformation may mask any surrounding topological expression and/or rockfall from higher up the dome may do likewise. There is another source of observations that is highly relevant to this problem, the rockfalls themselves. The location of rockfalls could shed light on whether deformation of the talus is localised, as is the case in shear-lobe dominated dome growth, or whether deformation of the talus is uniform, as might be the case for whole-dome endogenous growth. Rockfalls are measured routinely by the MVO seismometer network, with the frequency character, time, energy and duration of each event recorded (Luckett et al., 2002; Calder et al., 2005). These data can be used to build up an aggregate budget of events (e.g. Calder et al., 2005; Wadge et al., 2008a). We employ these rockfall data to test against the model in a companion paper (Hale et al. 2009).

Finally, does it matter whether we know about the disposition of the core/talus boundary and the size of these domains within siliceous lava domes? It certainly matters from a hazard analysis perspective. The more core lava that exists within a dome, in both relative and absolute terms, then the more explosive energy is available, both for large pyroclastic flows following collapse and particularly for lateral blast events following very rapid removal of lateral support to the dome. Knowledge of the location of the core lava within the dome is also significant for hazard assessment purposes. A spreading toe or lobe of core lava over a weak talus substrate may be both relatively unstable and likely to accelerate to more violent activity during the early phases of a retrogressive collapse (e.g. Herd et al., 2005). Such weak layers of talus that exist below malleable dome core may be prone to erosion and removal and it could be this mechanism which promotes catastrophic failure during heavy rainfall.

Acknowledgments: We thank the MVO staff who have been responsible for collecting the monitoring data, without which this study would not have been possible, as well as Sarah Ogburn at University at Buffalo for making Figure 4. Support is gratefully acknowledged from the Australian Research Council Discovery grant DP0771377 and AJH also acknowledges a University of Queensland Early Career Research Grant. ESC acknowledges NSF funding (Grant

Number 0809543) as well as a UB2020 Scholars grant. GW is supported by NERC grant NE/E015093/1. SCL publishes with permission of the Executive Director of BGS (NERC).

References:

Barclay, J., M. J. Rutherford & M. R. Carroll, 1998. Experimental phase equilibria constraints on pre-eruptive storage conditions of the Soufriere Hills magma, *Geophys. Res. Lett.*, **25**, 3437 - 3440.

Calder, E. S., Lockett, R., Sparks, R. S. J., & Voight, B., 2002, The eruption of Soufriere Hills Volcano, Montserrat from 1995 to 1999. *Geological Society, London Memoir*, **21**, 173–190.

Calder E. S., Cortes J. A., Palma J. L. & Lockett R., 2005. Probabilistic analysis of rockfall frequencies during an andesite lava dome eruption: The Soufriere Hills Volcano, Montserrat, *Geophysical Research Letters*, **32**, L16309

Carn, S. A., Watts, R. B., Thompson, G. & Norton, G. E., 2004. Anatomy of a lava dome collapse: the 20 March 2000 event at Soufrière Hills Volcano, Montserrat. *J. Volc. Geotherm. Res.*, **131**, 241 - 264.

Caricchi, L., Burlini, L., Ulmer, P., Gerya, T., Vassalli, M & Papale, P., 2007. Non-Newtonian rheology of crystal-bearing magmas and implications for magma ascent dynamics. *Earth and Planetary Science Letters*. **264**. 402 – 419.

Casagli, N., Tibaldi, A., Merri, A, Del Ventisette, C, Apuani, T, Guerri, L., Fortuny-Guasch, J., Tarchi, D. 2008. Deformation of Stromboli Volcano (Italy) during the 2007 crisis by radar interferometry, numerical modelling and field structural data. *J. Volcano. Geotherm. Res.*, (in review).

Cashmann, K. & J. Blundy, 2002. Degassing and crystallization of ascending andesite and dacite, *Phil. Trans. Royal Soc. Lon. A.*, **358**, 1487 - 1513.

Cole, P. D., Calder, E. S., Druitt, T. H., Hoblitt, R., Robertson, R., Sparks, R. S. J. & Young, S. R., 1998. Pyroclastic flows generated by gravitational instability of the 1996-97 lava dome of Soufriere Hills Volcano, Montserrat. *Geophysical Research Letters* 25, 3425 - 3428

Couch, S., Sparks, R. S. J., Carroll, M. R., 2003. The kinetics of degassing-induced crystallization at Soufriere Hills Volcano, Montserrat. *J. Petrol.* **44**, 1477 - 1502.

Gross, L., Bourgoin L, Hale A. J., & Mühlhaus H.-B., 2007. Interface Modeling in Incompressible Media using Level Sets in Escrip, *Physics Earth Planet. Int.*, **163**, 23–34

Hale, A. J., Calder, E. S., Loughlin, S., & Wadge, G., 2009. Modelling the Lava Dome Extruded at Soufriere Hills Volcano, Montserrat, August 2005 - May 2006. Part II: Rockfall Activity and Talus Deformation. (*submitted*)

Hale, A. J., Bourgoin L., & Mühlhaus H.-B. 2007. Using the level set method to model endogenous lava dome growth, *J. Geophys. Res.*, **112**, B03213 doi:10.1029/2006JB004445.

Hale, A. J., 2008. Lava Dome Growth and Evolution with an Independently Deformable Talus. *Geophysical Journal International*. **174**, 391–417

Hale, A. J. & Wadge, G., 2008. The transition from endogenous to exogenous growth of lava domes with the development of shear bands. *Journal of Volcanology and Geothermal Research*, **171**, 237–257.

Herd, R. A., Edmonds, M. & Bass, V. A., 2005. Catastrophic lava dome failure at Soufriere Hills Volcano, Montserrat, 12–13 July 2003, *J. Volc. Geotherm. Res.*, **148**, 234–252.

Hort, M., 1998. Abrupt change in magma liquidus temperature because of volatile loss or magma mixing: effects on nucleation, crystal growth and thermal history of the magma. *J. Petrol.*, **39**, 1063–1076.

Huppert, H. E., J. B. Shepherd, H. Sigurdsson, et al., 1982, On lava dome growth with application to the 1979 lava extrusion of the Soufriere St. Vincent. *J. Volcanol. Geotherm. Res.*, **14**, 199 - 222

Lavallée, Y., Hess, K.-U., Cordonnier, B. & Dingwell, D. B., 2007. Non-Newtonian rheological law for highly crystalline dome lavas. *Geology*, **35** 843 - 846

Loughlin, S. C., Baptie, B, Christopher, T., Ryan, G., Luckett, R., Hards, V., Jones, L., Fournier, N., Bass, V., Syers, T., Ruzie, L., Higgins, M., Williams, P & Williams, D., 2006. *Report to the Scientific Advisory Committee Montserrat, August 2006. MVO Open File Report 06/07.*

Loughlin, S. C., Christopher, T., Luckett, R., Jones, L., Baptie, B., 2007. Large volume dome collapse at the Soufrière Hills Volcano, Montserrat, 20 May 2006. *Geophysical Research Abstracts*. **9**, 11090.

Loughlin, S. C., Luckett, R., Christopher, T., Jones, L., Ryan, G., Druitt, T., Baptie, B., Carn, S., Hards, V. Unprecedented gas release from a large volume and rapid dome collapse at Soufriere Hills Volcano, Montserrat on 20 May 2006. *Journal of Volcanology and Geothermal Research*. (In prep).

Lube, G., Huppert, H. E., Sparks, R. S. J., Freundt, A., 2005. Collapse of two-dimensional granular columns. *Physical Review E*. **72**, 041301.

Luckett, R., Baptie, B. & Neuberg, J., 2002. The relationship between degassing and rockfall signals at Soufrière Hills Volcano, Montserrat. *Geological Society, London, Memoirs* **21**, 595 - 602.

Major J.J., Dzurisin, D., Schilling, S.P. & Poland M.P. Photogrammetric monitoring of sustained, complex growth of the 2004-2008 Mount St. Helens 1 lava dome using oblique terrestrial photography Major, D. (In review, submitted to *GRL*).

Matthews, A. J., Barclay, J., Carn, S., Thompson, G., Alexander, J., Herd, R. & Williams, C., 2002. Rainfall-induced volcanic activity on Montserrat. *Geophys. Res. Lett.*, **29** (13), 1644.

Melnik, O. E. & R. S. J. Sparks, 1999. Non-linear dynamics of lava dome extrusion. *Nature* **402**, 37-41.

Nicollin, F, Gibert. D, Beauducel, F., Boudon, G. & Komorowski, K., 2006. Electrical tomography of La Soufrière of Guadeloupe volcano: Field experiment, 1-D inversion, and qualitative interpretation. *Earth Planet. Sci. Lett.*, **244**, 709-724.

Simmonds, J., Elsworth D.& Voight B. 2005. Classification and idealized limit-equilibrium analyses of dome collapses at Soufrière Hills volcano, Montserrat, during growth of the first lava dome: November 1995–March 1998. *J. Volc. Geotherm. Res.*, **139**, 241–258.

Sparks, R. S. J., Young, S. R., Barclay, J., Calder, E. S., Cole, P., Darroux, B., Davies, M. A. et al. 1998. Magma production and growth of the lava dome of the Soufriere Hills Volcano, Montserrat, West Indies: November 1995 to December 1997. *Geophysical Research Letters* 25 3421 - 3424

Sparks, R. S. J., M. D. Murphy, A. M. Lejeune, R. B. Watts, J. Barclay & S. R. Young, 2000. Control on the emplacement of the andesitic lava dome of the Soufrière Hills Volcano, Montserrat by degassing-induced crystallisation. *Terra Nova*, **12**, 14 - 20.

Vallance, J.W., Schneider, D.J. & Schilling, S.P. Chapter 9: Growth of the 2004-2006 Lava-dome complex at Mount. St. Helens. In, A volcano rekindled: The Renewed Eruption of Mount St. Helens, 2004-2006. Edited by Sherrod, D., Scott, W.E., and Stauffer, P.H. U.S. Geological Survey Professional Paper 2008-XXX (in Press).

Wadge G, Macfarlane D. G., Robertson D. A. Hale, A. J., et al. 2005. AVTIS: A novel millimetre-wave ground based instrument for volcano remote sensing. *Journal of Volcanology and Geothermal Research*, **146**, 307-318.

Wadge, G., MacFarlane, D. G., Odbert, H. M., James, M. P., Hole, J. K., Ryan, G., Bass, V., De Angelis, S., Pinkerton, H., Robertson, D. A. & Loughlin, S. C., 2008. Lava dome growth and mass wasting measured by a time series of ground-based radar and seismicity observations. *Journal of Geophysical Research*, **113**, B08210, doi.1029/2007JB005466.

Wadge, G., 2009. Assessing the pyroclastic flow hazards at Soufriere Hills Volcano, Montserrat. In: *Advances in Volcanology: the Legacy of G.P.L.Walker*, Geol. Soc. London (in press).

Wadge, G., Ryan, G. & Calder, E. S., Clastic and core lava components of a silicic lava dome. *Geology* (In review).

Watts, R. B., R. A. Herd, R. S. J. Sparks & S. R. Young, 2002. Growth patterns and emplacement of the andesitic lava dome at Soufrière Hills Volcano, Montserrat, *Geological Society, London Memoir*, **21**, 115 - 152.

Wu, Y. C., Thompson, E. G. & Heylinger, P. R., 2003. The compaction of aggregates of non-spherical linear viscous particles. *Comput. Methods Appl. Mech. Engrg.* **192**, 4929 - 4946.

Wu, Y. C., Thompson, E. G., Heylinger, P. R. & Yao, Z., 2004. The compaction of blended aggregates of non-spherical linear viscous particles. *Comput. Methods Appl. Mech. Engrg.* **193**, 3871 - 3890.

Figure captions:

Figure 1: Photo of the lava dome extruded at Soufrière Hills Volcano on 18th May 2006 looking towards the southwest, reproduced with permission of the Montserrat Volcano Observatory. This photo was taken during a period of endogenous inflation, manifested by the regular fractured structure of the blocks in the central region of the dome. Copyright NERC/Government of Montserrat.

Figure 2: Boundary conditions used in the model. The model domain has an axis of symmetry about $r = 0$ and this allows us to only model a 2D slice, reducing computing solving time. The base of the domain has the boundary conditions of no-slip (as shown by the fixed triangle symbol), the axis of symmetry at $r = 0$ permits flow only in the z -direction (shown by the triangle on rollers), while the boundaries away from $r = 0$ and $z = 0$ are open and allow matter to flow in/out of the domain. Magma is introduced into the model domain through a conduit with radius a . The free-surface of the dome and the core-talus interface are described by level-sets.

Figure 3: Surveyed cumulative dome volume data (crosses) and best-fit to dome volume with time (continuous line). Also shown on the secondary y -axis is the extrusion rate derived from the best-fit curve for the volume (dashed line), and the extrusion rate interpolated from the surveyed volume-time data (filled circles).

Figure 4: Slope map for the SHV lava dome during April 2007, derived from the digital elevation map of the dome, created by Sarah Ogburn at University at Buffalo. Although this is, a different eruptive time period to the one considered in this paper, this slope map is provided because the dome shape was particularly well-constrained during this period, and shape, and in particular the talus angle of repose is considered typical for other periods. Slope angles are given in degrees and are contoured in 10-degree intervals. The majority of the upper slope of the dome sits in the range 31-40 degrees, with maximum slopes on the south-eastern side reaching 41-50 degrees. Note that the dome was somewhat flat-topped during this period.

Figure 5: Simulated lava dome free-surface on 30th March and 7th April 2006 as shown by the continuous coloured lines as described in Table 3. Also shown is the free-surface imaged by

Wadge et al. (2008) on these dates as continuous and dashed thick black lines. This conduit exit centre at the Montserrat coordinates 380919 and 1847090. All the images show the free-surface of the lava dome from $r = 0$, the conduit exit, to the lateral extent of the dome. The base of the dome model at a height of 0 metres is equivalent to an elevation of 680 m asl .

Figure 6: Maximum height and radius of the simulated lava domes as described in Table 2. Also shown are observational data points, red data points are taken from Wadge et al. (2008) while black points are from the Montserrat Volcano Observatory survey data.

Figure 7: Three-dimensional images of the dome with segments left out to observe the interior structure produced by Simulation 2 that uses a shear-thinning viscosity relationship (Lavallée et al., 2007), a friction angle of 43.5° and a solidus pressure of 0.4 Mpa. The four images show the dome core (light grey) and talus (dark grey) representing the structure at different dates: a) 1st October 2005 (48 days), b) 1st December 2005 (109 days), c) 1st February 2006 (171 days) and d) 1st April 2006 (230 days).

Figure 8: a) Schematic of the lava dome model during the talus adjustment sub-step. Following the new injection of lava, the smallest radius from the centre of the dome, R_a , where the dome is unstable, and hence where the talus needs to be adjusted to rest at its angle of repose is calculated. The talus source volume corresponds to the domain that is occupied by talus or carapace before the gravity readjustment phase (i.e. prior to the unstable region of talus being adjusted to rest at the angle of repose), minus the area of the domain that is now occupied by talus directly following the talus readjustment sub-step, integrated about 2π and divided by the time-step duration. b) shows a simulated lava dome free-surface (grey lines) and core-talus interface (black lines) for the dates: 1 Oct. 2005, 1 Dec. 2005, 1 Feb. 2006, 1 Mar. 2006 and 20 May 2006. The shaded region of talus that can be better classified as carapace as given in the model by R_a and H_a .

Figure 9: Lava dome surface and core-talus interface growth plots. For the plots on the left, the black continuous lines correspond to the core-talus interface, while the grey continuous lines correspond to the free-surface of the dome. The lines correspond to the dates: 1 Oct. 2005, 1

Dec. 2005, 1 Feb. 2006, 1 Mar. 2006 and 20 May 2006. The plots on the right show the location on the free-surface for the point at which the talus departs from the angle of repose, i.e. R_a and H_a , the height of the dome at R_a expressed as grey points. A black solid line is used to guide the eye to show H_a and c change as the dome grows and the red points correspond to observational data as described in the text. The figures correspond to the simulations described in Table 1: a) Simulation 1, b) Simulation 2, c) Simulation 3, d) Simulation 4, e) Simulation 5, f) Simulation 6, g) Simulation 7, and h) Simulation 8.

Figure 10: Velocity field at a time of approximately 261 days for Simulation 3, i.e. a shear thinning viscosity relationship, friction angle equal to 43.5° and a solidus pressure of 0.6 MPa. Arrows correspond to the direction of the velocity field, but not the magnitude. The colour bar corresponds to the magnitude of the velocity, with pink being the highest and white the lowest. Note that the velocity scale is not linear. The inner black line shows the core-talus interface and the outer black line shows the free surface of the dome. Note that using the level-set technique we also model the air in this simulation but with a significantly lower viscosity (Hale et al., 2007).

Figure 11: Simulated core-talus interfaces (a) and final dome free-surfaces (b) on 20th May 2006 for the simulations considered. The key on the left corresponds to the Simulation described in Table 2. c) shows all the simulated free-surfaces (grey lines) and core-talus interfaces (black lines) on 20th May 2006.

Figure 12: Cumulative core volume fraction (core volume divided by dome total volume) with time for all simulations (Table 2).

Tables:

Table 1: A summary of the parameters values and ranges used for the simulations.

Parameter	Range	Value used	Reference
θ (Friction angle)	33 – 43.5°	37 – 43.5°	Wadge et al. (2008a)
ρ (Density)		2350 kg m ³	
r_a (Conduit radius)		15m	
P_s (Solidus pressure)	0.2 M Pa - 15 M Pa	0.2 M Pa – 0.6 M Pa	
T (Temperature)	830±10°C in magma chamber	830°C	Barclay et al., (1998)

Table 2: Simulations modelled.

Simulation	Viscosity model	Friction angle	Solidus pressure
1	Shear-thinning viscosity relationship (Lavallée et al., 2007) with strain-rate cut-off of 10^{-5} s^{-1} .	43.5°	0.2MPa
2	Shear-thinning viscosity relationship (Lavallée et al., 2007) with strain-rate cut-off of 10^{-5} s^{-1} .	43.5°	0.4MPa
3	Shear-thinning viscosity relationship (Lavallée et al., 2007) with strain-rate cut-off of 10^{-5} s^{-1} .	43.5°	0.6MPa
4	Shear-thinning viscosity relationship (Lavallée et al., 2007) with strain-rate cut-off of 10^{-5} s^{-1} .	40.0°	0.4MPa
5	Shear-thinning viscosity relationship (Lavallée et al., 2007) with strain-rate cut-off of 10^{-5} s^{-1} .	37.0°	0.4MPa
6	Shear-thinning viscosity relationship (Lavallée et al., 2007) with strain-rate cut-off of 10^{-5} s^{-1} for the core, and a viscosity of $3.4 \times 10^{13} \text{ Pa s}$ for the talus.	43.5°	0.4MPa
7	Shear-thinning viscosity relationship (Lavallée et al., 2007) with strain-rate cut-off of 10^{-5} s^{-1} for the core, and a viscosity of 10^{14} Pa s for the talus.	43.5°	0.4MPa
8	Newtonian viscosity relationship, $3.4 \times 10^{12} \text{ Pa s}$.	43.5°	0.4MPa

Table 3: Key for Figure 5.

Image	Models	Line colour in Fig. 5
		5

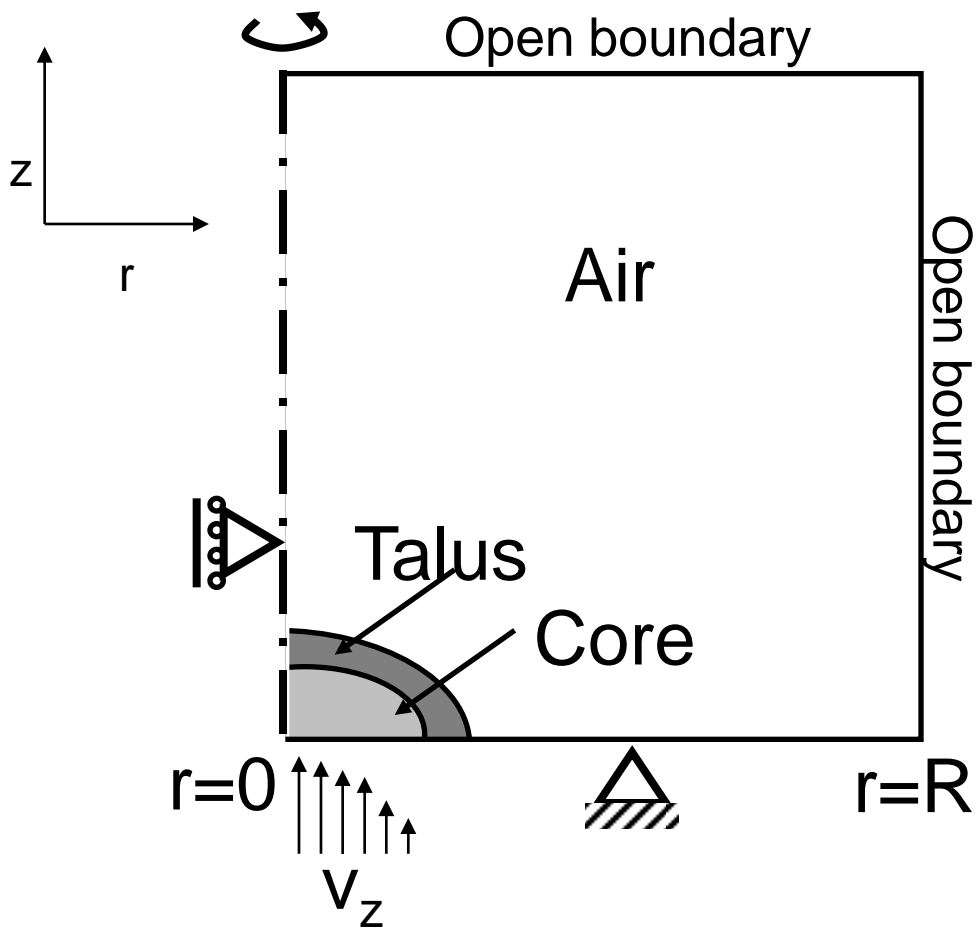
a	Shear-thinning viscosity relationship (Lavallée et al., 2007), Friction angle = 43.5°, Ps = 0.4 MPa.	Blue
	Newtonian viscosity model. Friction angle = 43.5°, Ps = 0.4MPa.	Red
b	Shear-thinning viscosity relationship (Lavallée et al., 2007), Friction angle = 43.5°, Ps = 0.4 MPa.	Blue
	Shear-thinning viscosity relationship (Lavallée et al., 2007), Friction angle = 40.0°, Ps = 0.4 MPa.	Red
	Shear-thinning viscosity relationship (Lavallée et al., 2007), Friction angle = 37.0°, Ps = 0.4 MPa.	Green
c	Shear-thinning viscosity relationship (Lavallée et al., 2007), Friction angle = 43.5°, Ps = 0.4 MPa.	Blue
	Shear-thinning viscosity relationship (Lavallée et al., 2007), Friction angle = 43.5°, Ps = 0.2 MPa.	Red
	Shear-thinning viscosity relationship (Lavallée et al., 2007), Friction angle = 43.5°, Ps = 0.6 MPa.	Green
d	Shear-thinning viscosity relationship (Lavallée et al., 2007), Friction angle = 43.5°, Ps = 0.4 MPa.	Blue
	Shear-thinning viscosity relationship (Lavallée et al., 2007) with a 10 times higher viscosity in the talus. Friction angle = 43.5°, Ps = 0.4 MPa.	Red

Figure 1
[Click here to download high resolution image](#)

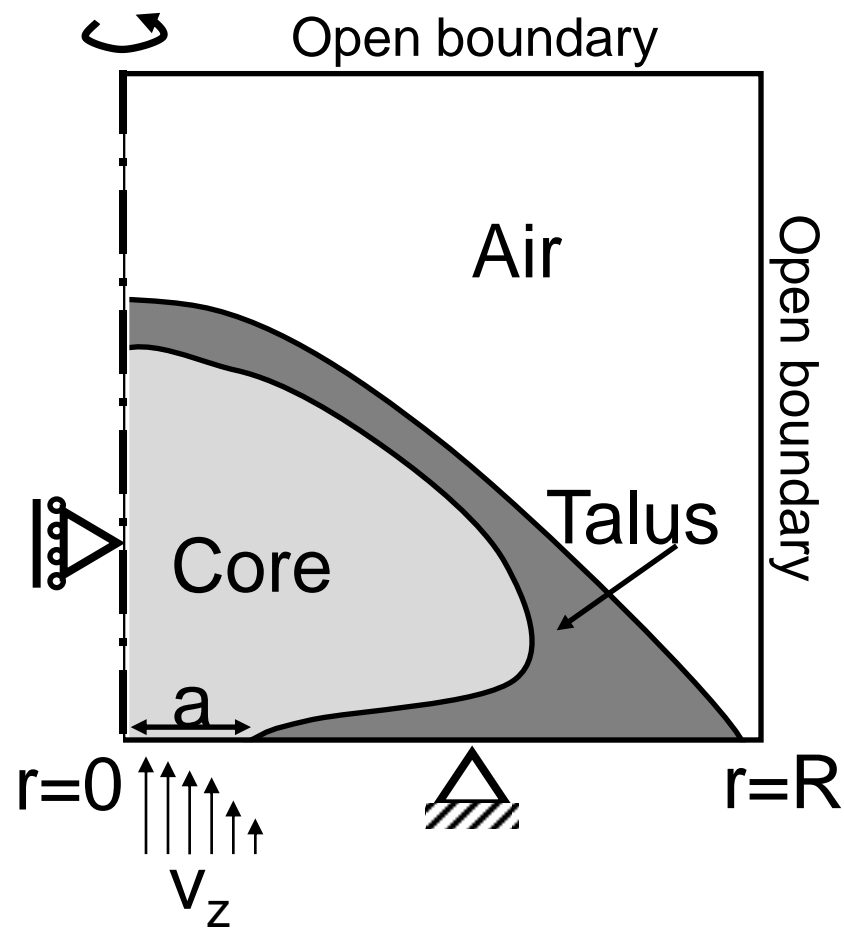


Figure 2

[Click here to download Figure: ModelSetUp.pdf](#)



Initial condition



Model after n time-steps

Figure 3
[Click here to download high resolution image](#)

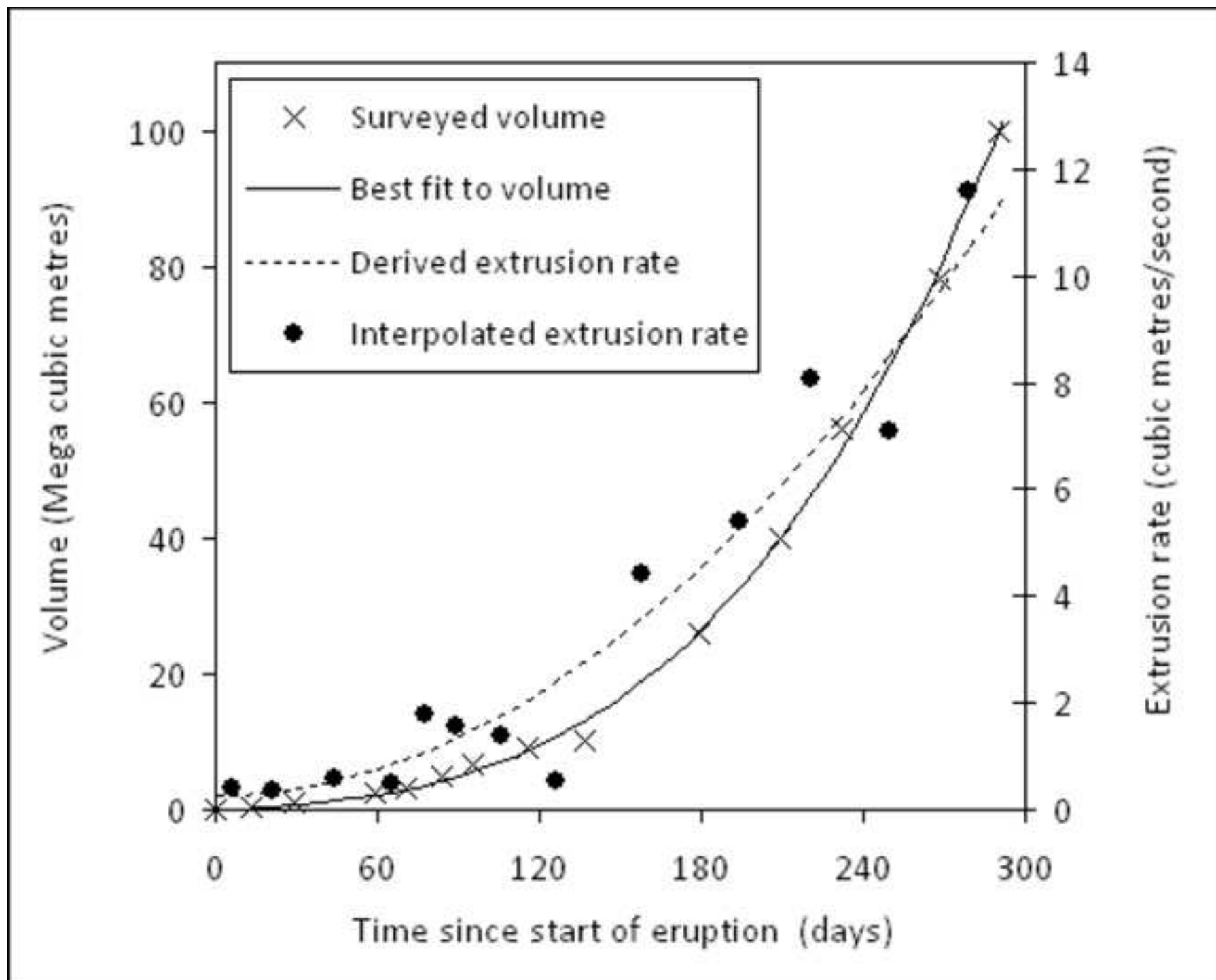


Figure 4
[Click here to download high resolution image](#)

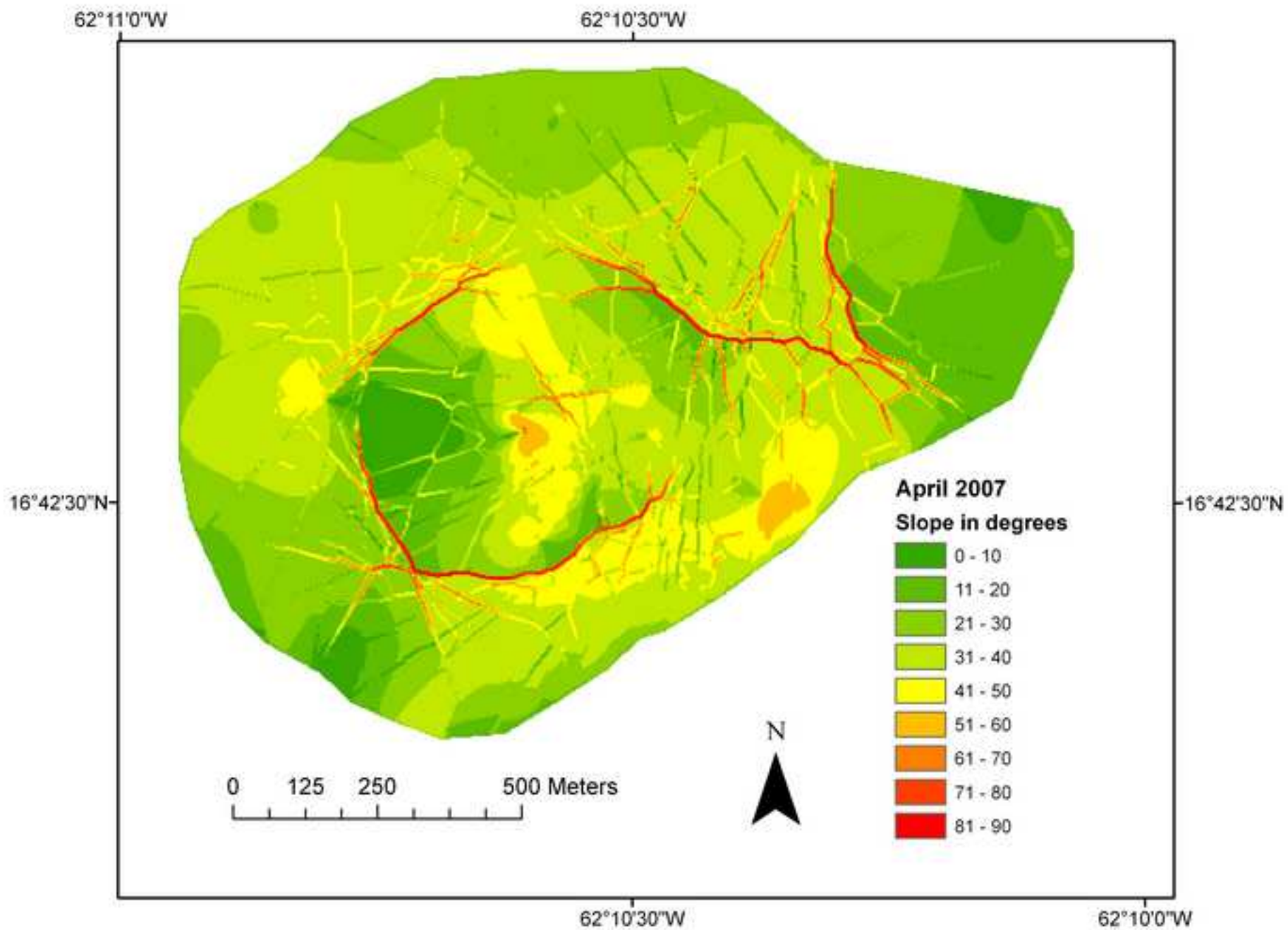
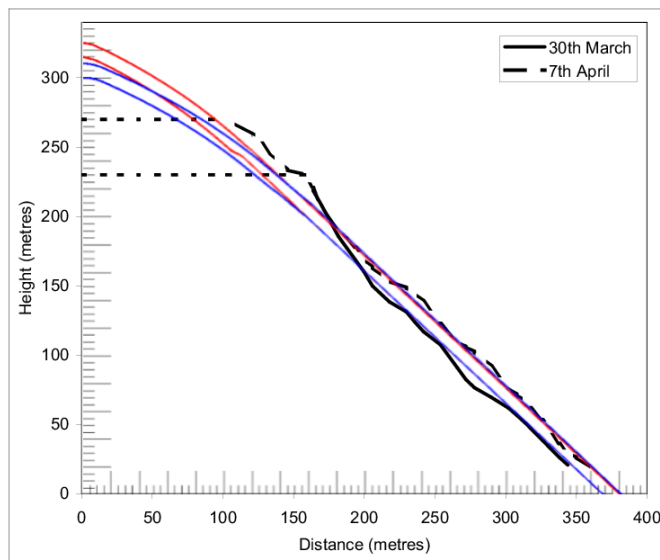
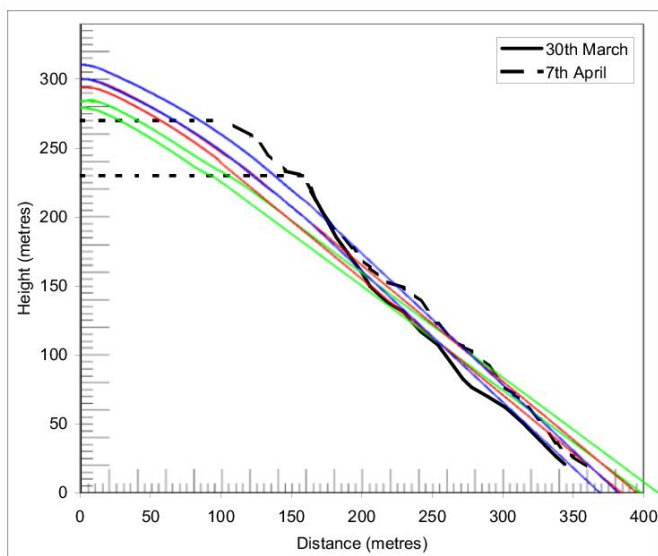


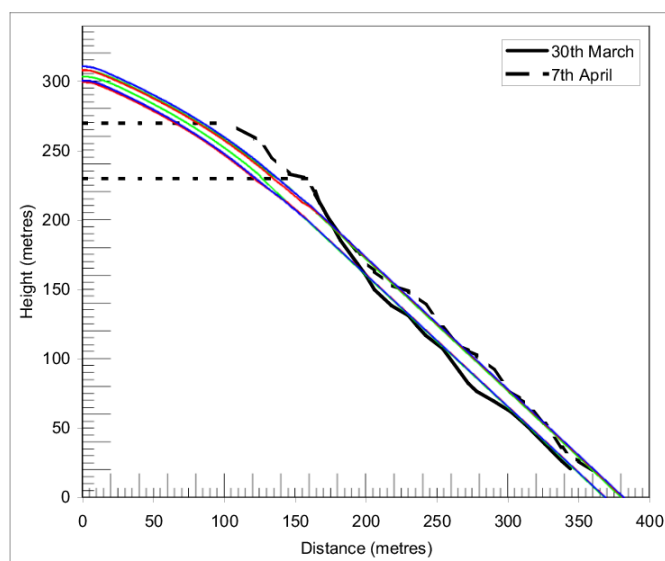
Figure 5:



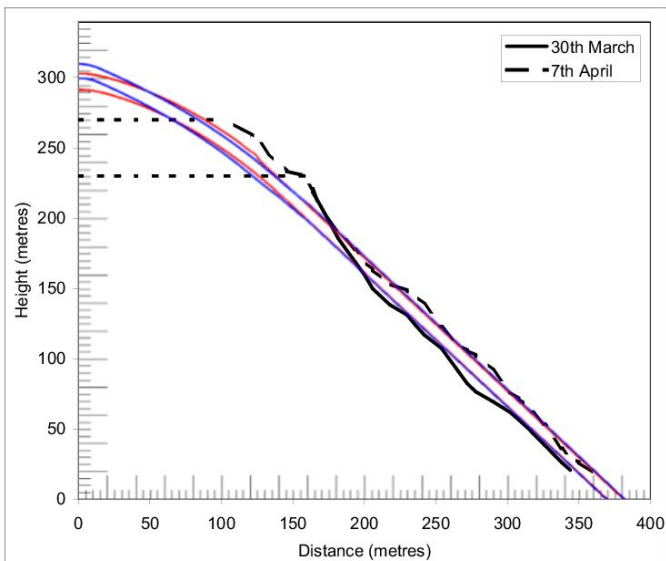
a)



b)

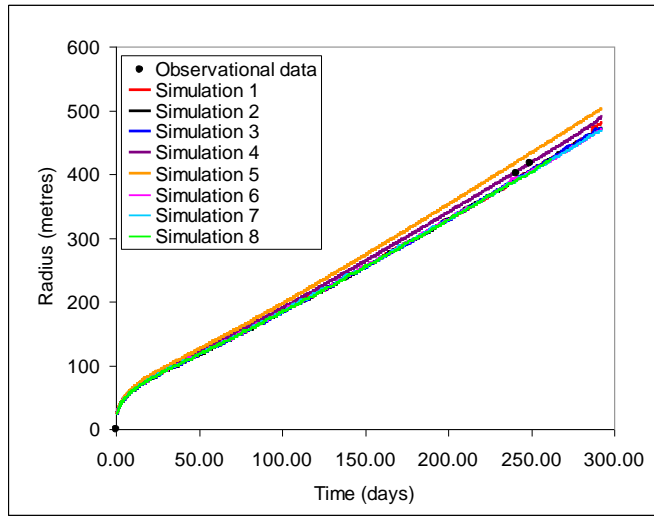


c)

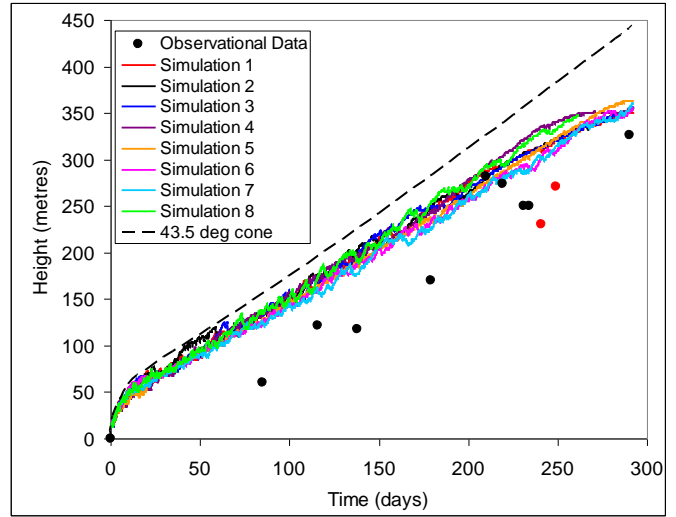


d)

Figure 6:



a)

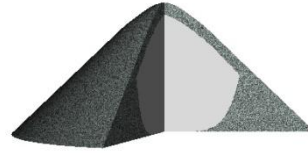


b)

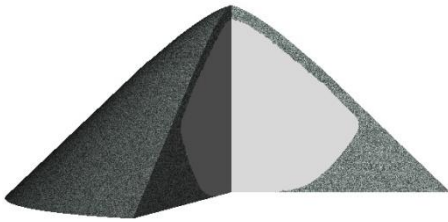
Figure 7:



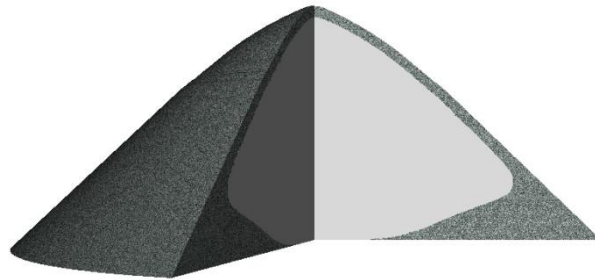
a) 1st October 2005 (48 days)



b) 1st December 2005 (109 days)

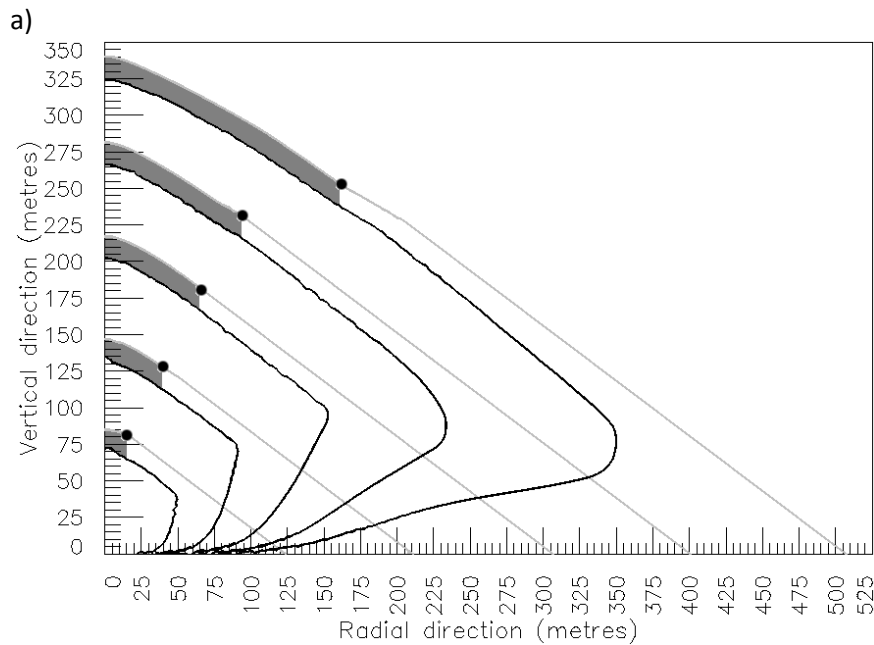
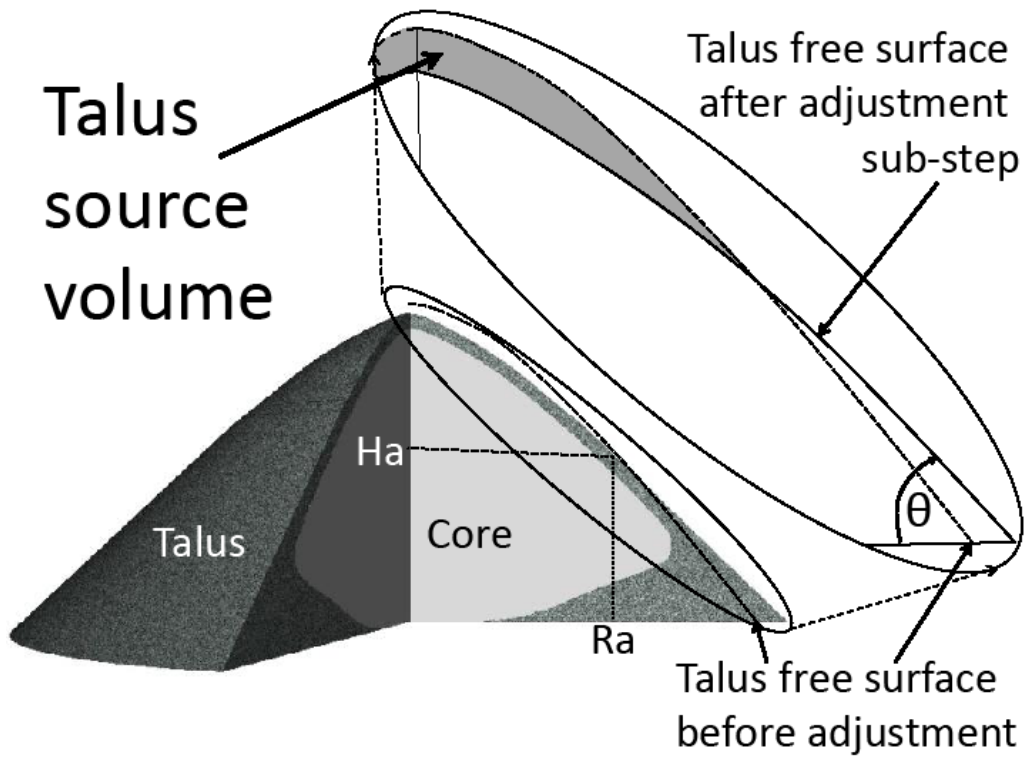


c) 1st February 2006 (171 days)



d) 1st April 2006 (230 days)

Figure 8:

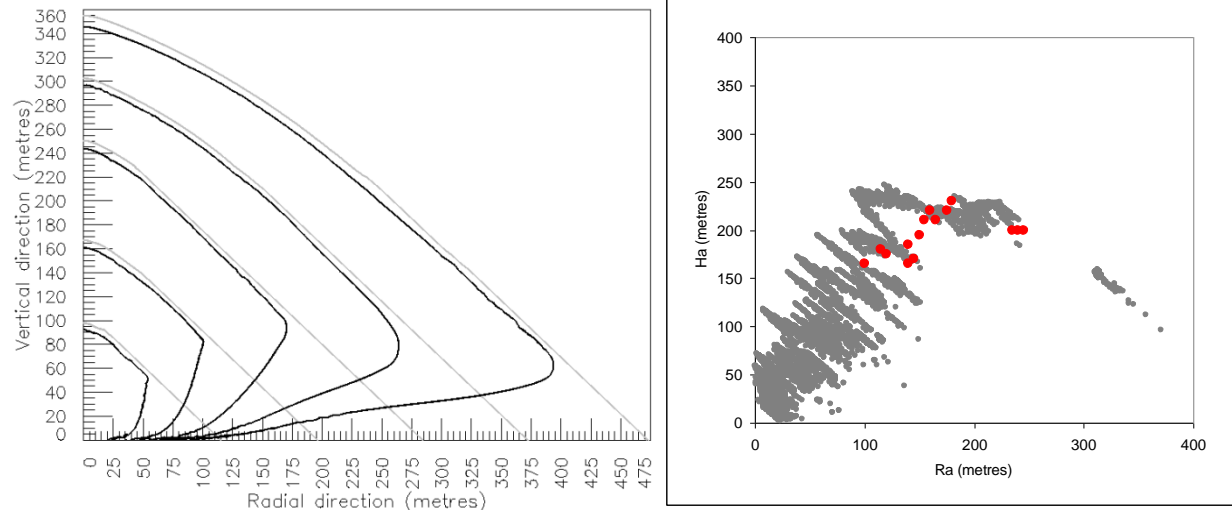


b)

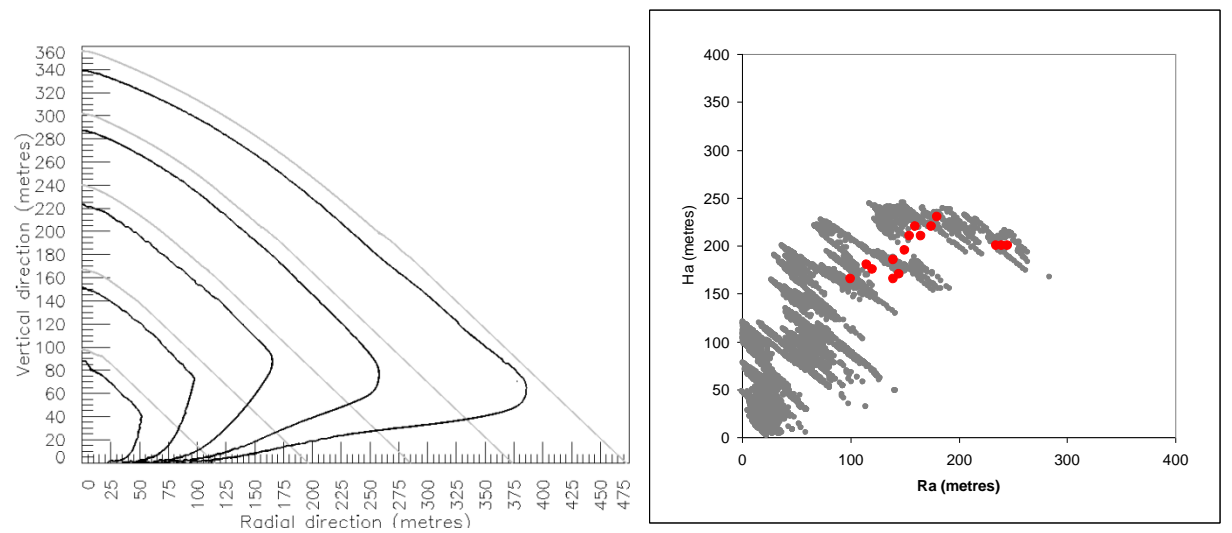
Figure 9

[Click here to download Figure: Figs9.pdf](#)

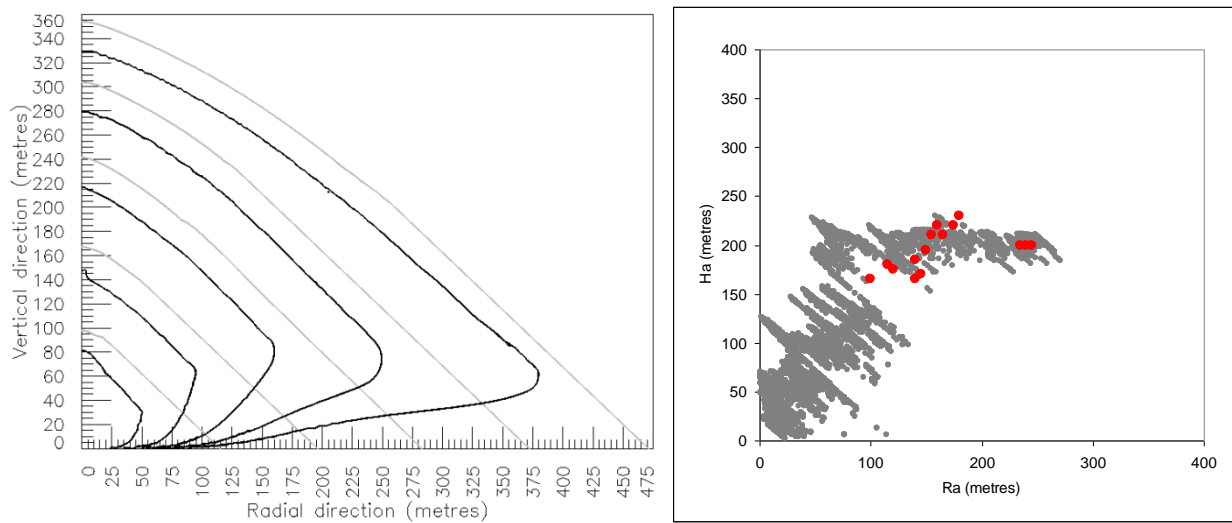
Figure 9:



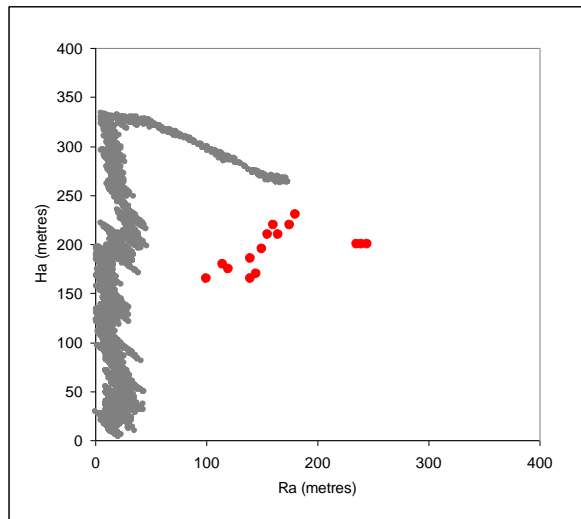
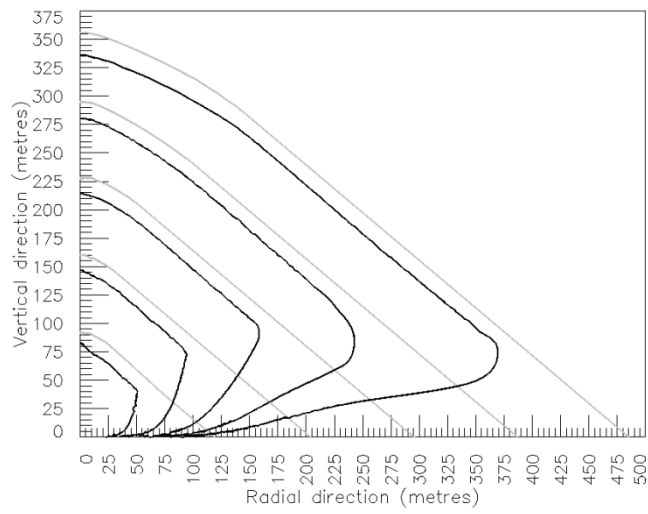
a) Simulation 1



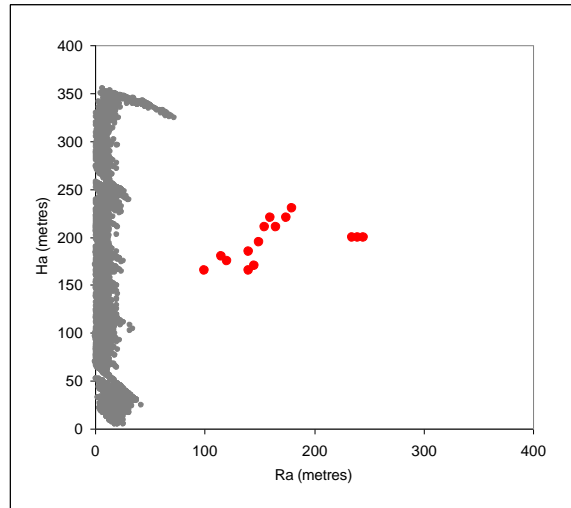
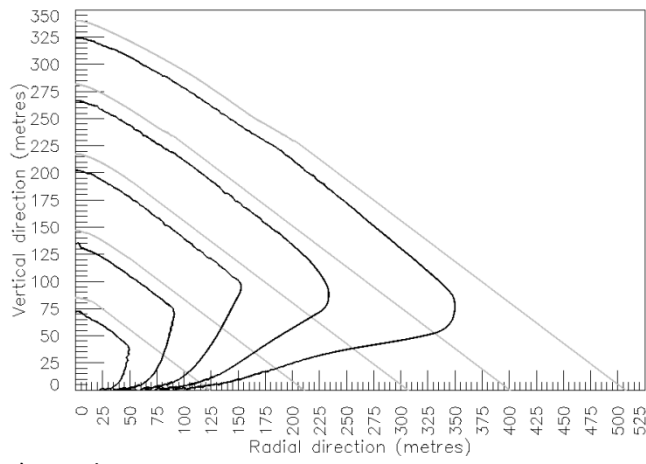
b) Simulation 2



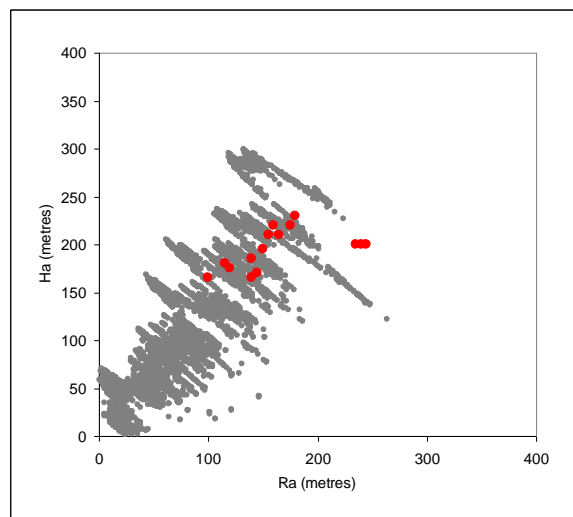
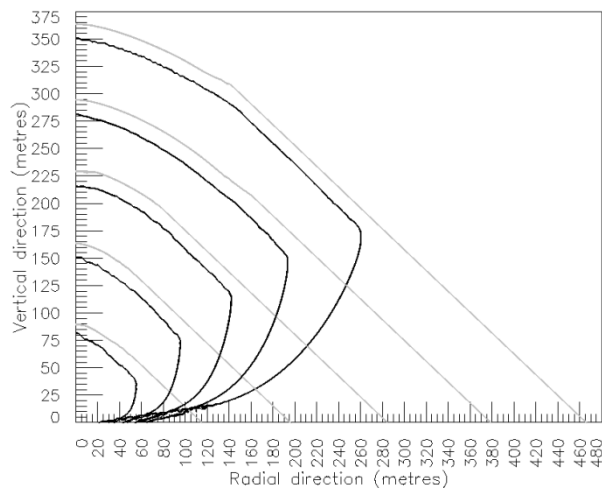
c) Simulation 3



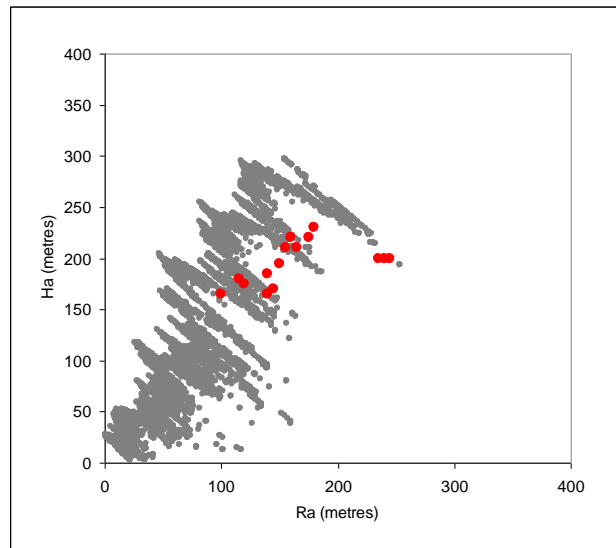
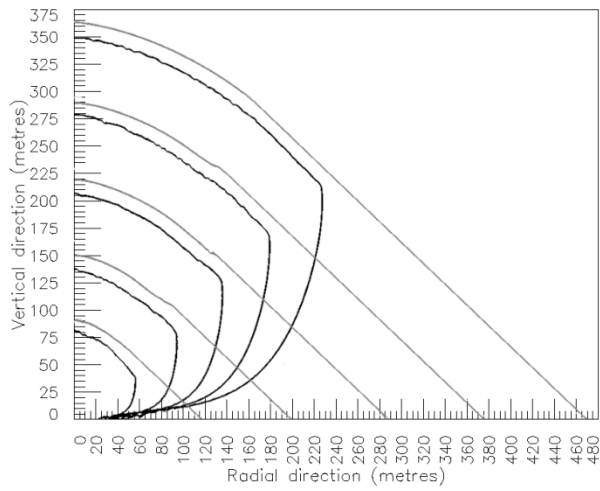
d) Simulation 4



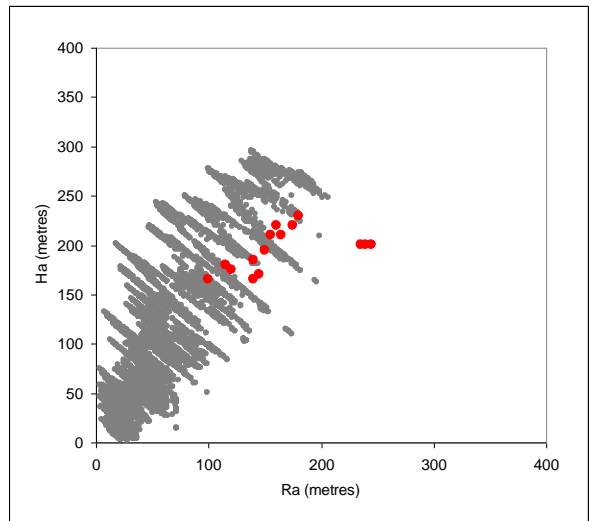
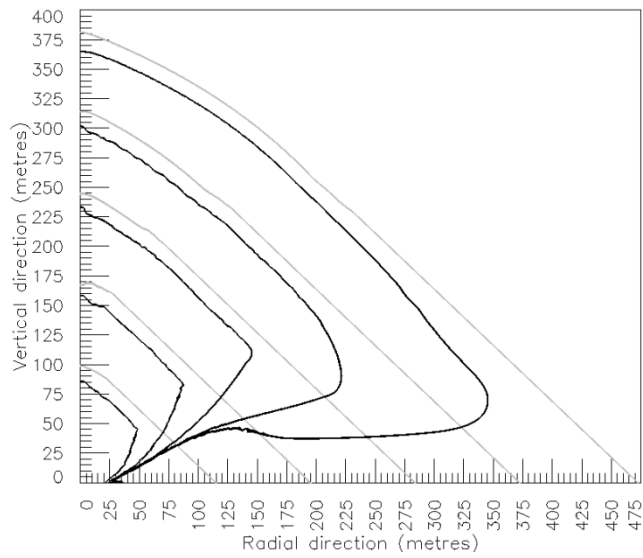
e) Simulation 5



f) Simulation 6



g) Simulation 7



h) Simulation 8

Figure 10
[Click here to download high resolution image](#)

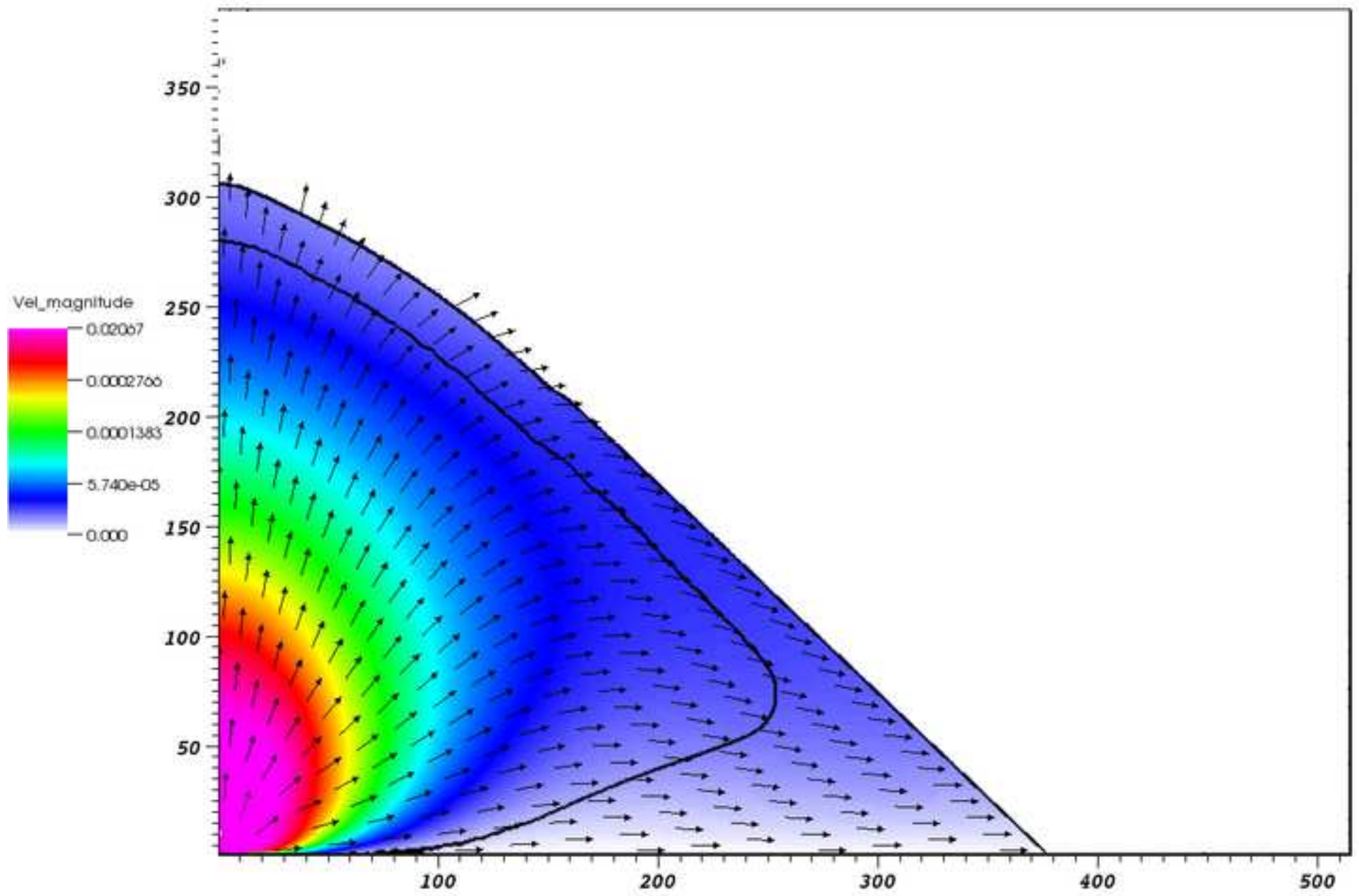
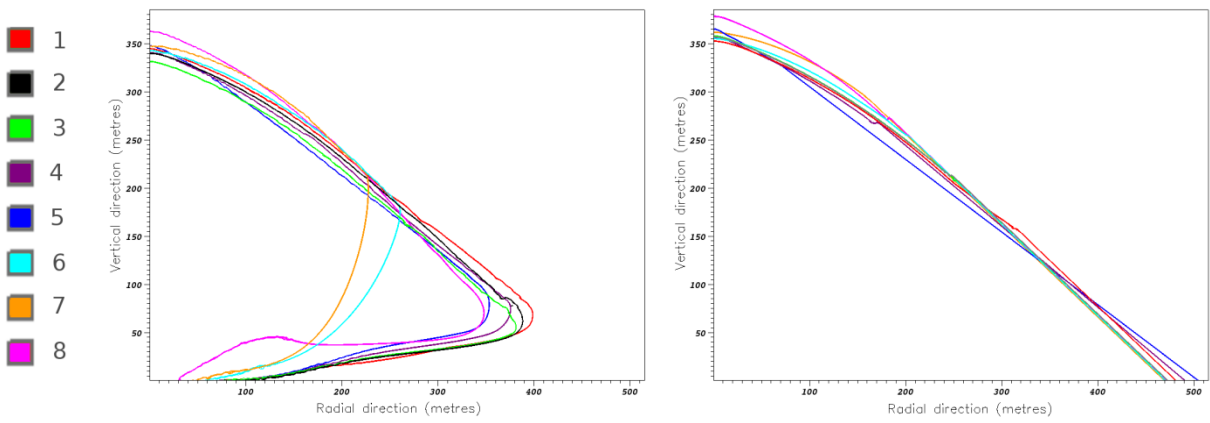


Figure 11

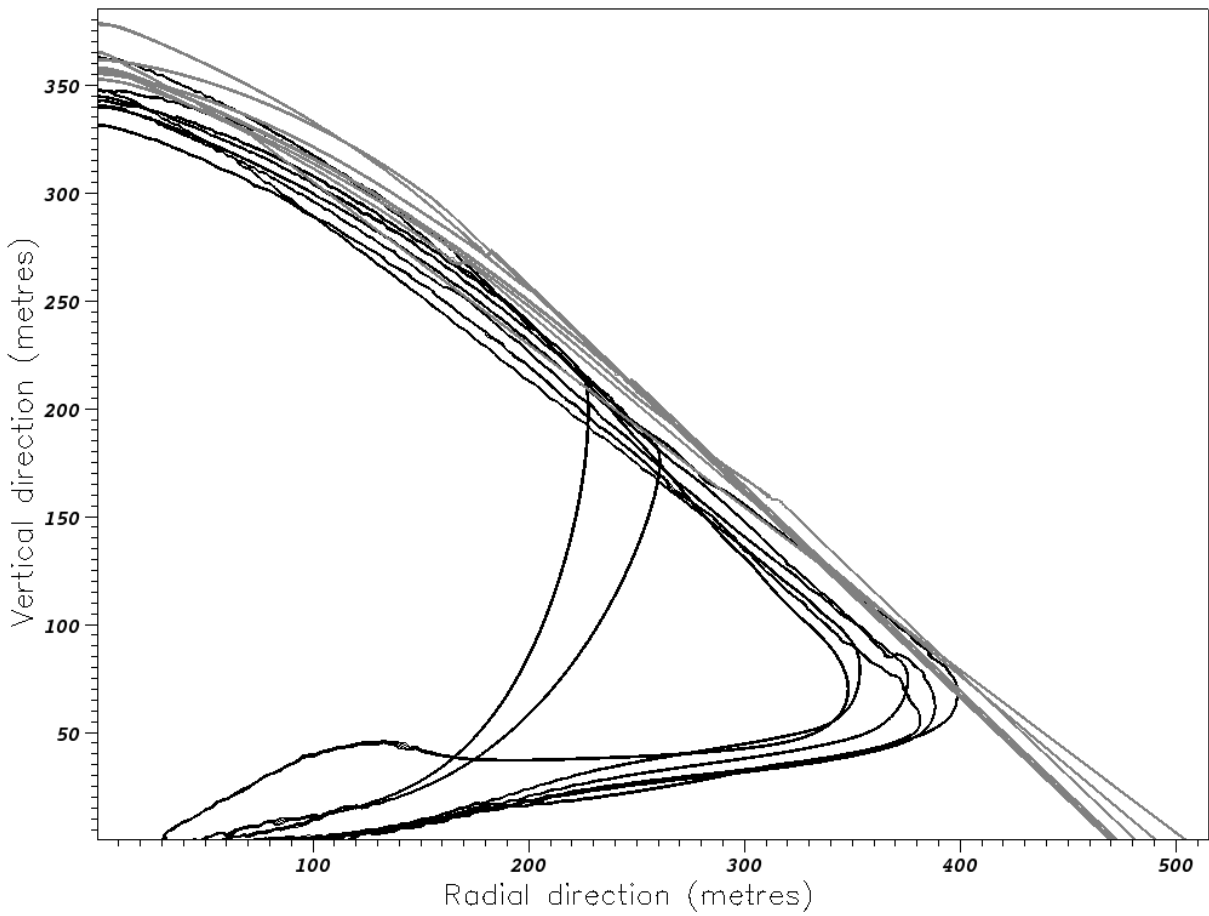
[Click here to download Figure: Fig11.pdf](#)

Figure 11:



a)

b)



c)

Figure 12
[Click here to download high resolution image](#)

